Nonlinear spectroscopy in the strong-coupling regime of cavity QED

R. J. Thompson,* Q. A. Turchette,† O. Carnal,‡ and H. J. Kimble
Norman Bridge Laboratory of Physics, California Institute of Technology, Pasadena, California 91125

(Received 10 June 1997; revised manuscript received 9 December 1997)

A nonlinear spectroscopic investigation of a strongly coupled atom-cavity system is presented. A two-field pump-probe experiment is employed to study nonlinear structure as the average number of intracavity atoms is varied from $\bar{N}\approx 4.2$ to $\bar{N}\approx 0.8$. Nonlinear effects are observed for as few as 0.1 intracavity pump photons. A detailed semiclassical simulation of the atomic beam experiment gives reasonable agreement with the data for $\bar{N}\gtrsim 2$ atoms. The simulation procedure accounts for fluctuations in atom-field coupling which have important effects on both the linear and nonlinear probe transmission spectra. A discrepancy between the simulations and the experiments is observed for small numbers of atoms ($\bar{N}\lesssim 1$). Unfortunately, it is difficult to determine if this discrepancy is a definitive consequence of the quantum nature of the atom-cavity coupling or a result of the severe technical complications of the experiment. [S1050-2947(98)09704-2]

PACS number(s): 42.50.Fx, 32.80.−t, 42.65.−k

I. INTRODUCTION

An exciting development in recent years has been the experimental investigation of open quantum systems in the domain of strong coupling. In this limit the time scale for internal, coherent evolution of a quantum system is much shorter than the time scale for dissipation into an external environment [1]. Increasing the ratio of coherent coupling to dissipation is of primary import in many nascent fields of experimental quantum physics including quantum computation [2] and quantum state synthesis [3–6]. Experimental examples of such systems are scarce, with notable exceptions being photon-phonon coupling in trapped ion systems [7] and photon-atom coupling in the field of cavity quantum electrodynamics (cavity QED). Strong-coupling cavity QED experiments have been carried out in both the microwave [8–15] and optical domains [1,16–22].

Thus far, most experiments in strong-coupling cavity QED with few atoms which have focused on structural properties (eigenstructure) of the coupled system have been performed in the linear regime. It has been pointed out numerous times [1,17,22–27] that the linear regime is equally well described by the semiclassical Maxwell-Bloch equations or by a full quantum master equation. As regards *structural* aspects of the coupled system, only (nonlinear) excitations of high-lying dressed states can potentially distinguish between theories. Recently, in the microwave domain, peaks arising from such a nonlinear excitation have been observed in the Fourier transform of a time-domain Rabi oscillation [28]. Alternative to structural aspects of the atom-cavity interaction are measurements of *dynamical* processes such as photon antibunching [16] and sub-Poissonian photon statistics [10] for which a manifestly quantum theory of strong coupling in cavity QED is required.

In order to advance spectroscopic investigations in optical cavity QED from the classical (linear) domain to the quantum regime, we have carried out both linear and nonlinear optical spectroscopic measurements of a strongly coupled atom-cavity system with average intracavity atom number ranging from $\bar{N}\approx 4.2$ to $\bar{N}\approx 0.8$. In particular, we have observed with significantly improved resolution over our previous results [17] a weak-field normal-mode (or ‘‘vacuum-Rabi’’) splitting of the transmission spectrum of the coupled system [1,20]. Moreover, we have recorded modifications of weak-field spectra in the presence of a moderate intensity pump field of fixed frequency. Significant nonlinear effects were observed with as few as 0.1 intracavity photons. This investigation complements our measurements of nonlinear response in the bad-cavity limit of cavity QED [29], where we have studied a quantum-phase gate for quantum logic with saturation photon number 0.02 [30].

A principle motivation for this research is the identification (in the level structure of the atom-cavity ‘‘molecule’’) of manifestly quantum aspects of the atom-cavity interaction. In particular we have attempted to observe multiquanta transitions, using a pump-probe technique in which the system is driven to its first excited state using a fixed-frequency pump field, with transitions to higher-lying states probed by a weak, variable-frequency probe field. With on average less than one atom in the cavity-mode volume, deviations from a semiclassical model are observed, but an unambiguous signature of a multiexcitation resonance of uniquely quantum origin remains elusive to the experiments described here.

It must be noted at the outset that this experiment along with almost all strong-coupling atomic cavity QED work to date is performed with an atomic beam which crosses the cavity mode (the exception is Ref. [31]). Because of this, the effects of fluctuations in atomic number inherent in the beam, along with spatially variant coupling strength within the cavity, play an extremely important role in the interpre-

---

*Present address: Jet Propulsion Laboratory, California Institute of Technology, M/C 298-100, Pasadena, CA. Electronic address: rjthomp@horology.jpl.nasa.gov

†Present address: National Institute of Standards and Technology, Division 847, Boulder, CO 80303. Electronic address: quentint@boulder.nist.gov

‡Present address: Holtronics Technologies, Champs-Montants 12b, CH-2074 Marin, Switzerland.

tation of observations. While this has been stressed in our previous work [16–19], which has included detailed quantitative comparisons based on a Monte Carlo simulation accounting for the effects of these fluctuations, the present nonlinear experiment with larger coupling raises new issues which we likewise address in detailed simulations of this experiment. The complicating effects of atomic beam fluctuations have also been considered theoretically in the work of Carmichael and co-workers [32,33]. There it was found that an approach alternative to the spectra measurements reported here— namely, a two-photon correlation technique—can provide rather clear signatures of the higher-lying Jaynes-Cummings levels even in the presence of atomic beam fluctuations. The experiments proposed there, while quite promising, add a level of additional technical complexity over the relatively simple measurements of transmission spectra employed here.

The organization of this article is as follows. In Sec. II we formulate the relevant theory and then in Sec. III we discuss methodology and results of our semiclassical simulations. Our measurements are discussed in Sec. IV. We conclude in Sec. V with a discussion of future techniques for improving measurements in cavity QED.

II. QUANTUM AND SEMICLASSICAL THEORY OF THE ATOM-CAVITY SYSTEM

A. Preliminaries: Structure of the atom-cavity system

The quantum mechanical structure of a dissipationless, strongly coupled atom-cavity system (in the absence of number fluctuations) is well known. The single-atom prediction is a spectrum of eigenvalues given by the so-called Jaynes-Cummings ladder [34]; an extension to the multiple-atom case is the Tavis-Cummings ladder [35] of dressed states. The formidable task of incorporating small amounts of dissipation in the system (via a master equation or other approach) reveals many interesting quantum mechanical effects (such as photon antibunching in the transmitted light [16,36]) and indicates that in the strong-coupling regime, the overall structure cannot be viewed in the absence of a self-consistent treatment of the nature of the complete interaction *including dissipation* [37]. Semiclassically, the problem has been treated from various perspectives, notably the state equation of optical bistability [38] derived either from the standard Maxwell-Bloch equations [39] or from the full master equation in a system size expansion [40]. Comparisons of the fully quantum and semiclassical approaches indicate that for two limiting cases predictions of the structure of the lowest-lying dressed states coincide. These are the limit of vanishing excitation strength and the limit of large numbers of intracavity atoms [41].

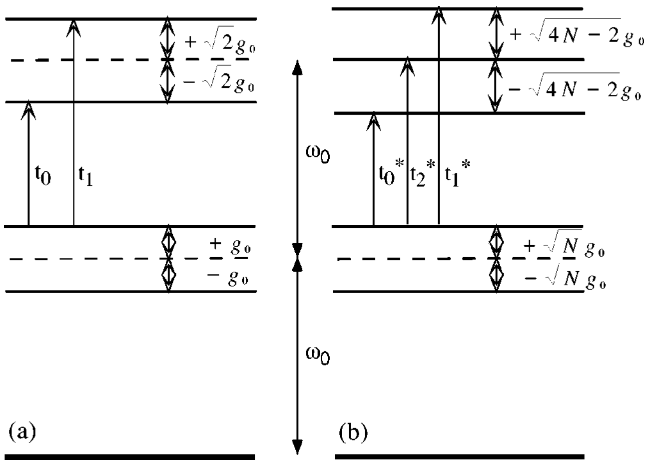

FIG. 1. Comparison of the level structure of the first two excited states of a coupled atom-cavity system for the one-atom case (left) and the many-atom case ($N>1$) (right). The transitions t_0 and t_1 occur at $-(\sqrt{2}+1)g_0$ and $+(\sqrt{2}-1)g_0$, respectively (relative to $\omega_0 \equiv \omega_a = \omega_c$). For $N \gg 1$, transitions t_0^*, t_1^*, and t_2^* are at $-3g_0\sqrt{N}$, $+g_0\sqrt{N}$, and $-g_0\sqrt{N}$ and t_0^* is highly suppressed, so that the first- to second-excited-state transitions overlap with the ground- to excited-state transitions, and the quantum anharmonicity is lost. By contrast, for one atom, there is a distinct separation between ground to first-excited-state and first- to second-excited-state transitions. Here, $\omega_A = \omega_c \equiv \omega_0$ with frequency offsets quoted relative to ω_0.

Figure 1 helps to explain the situation. Figure 1(a) depicts the first two excited states of a single atom optimally coupled to a cavity as derived from a full quantum calculation in which g_0 is the rate of coherent coupling between atom and cavity: $2g_0 \equiv \Omega_{\text{Rabi}}$, with Ω_{Rabi} the one-photon Rabi frequency. Figure 1(b) is the fully quantum extension of the one-atom calculation to the case with N atoms [41]. The exact quantum expression for the first-excited-state splitting is $g_0\sqrt{N}$ and that of the second excited state is $\pm g_0\sqrt{4N-2}$. For $N \gg 1$ the splitting of the excited state becomes $\pm 2g_0\sqrt{N}$, and transitions from the first to the second manifold occur at a frequency $\pm g_0\sqrt{N}$ in agreement with the semiclassical prediction. Note that the semiclassical prediction fails for small N both in terms of level splitting and transition strength. For weak-field excitation, the second excited state is never reached, so that the semiclassical and quantum predictions coincide. The quantum character of the second-excited-state splitting can be expressed in terms of a ‘‘quantum anharmonicity’’ which can be quantitatively defined as the ratio of the second-excited-state splitting for the quantum and semiclassical predictions:

$$q_a \equiv \frac{g_0\sqrt{4N-2}}{2g_0\sqrt{N}}. \tag{1}$$

For $N=1$, $q_a = 0.71$, while for $N \to \infty$, $q_a \to 1$.

Alternatively, we can examine the transition frequency δ_1 corresponding to t_1^* given by

$$\begin{aligned}\delta_1 &= g_0\sqrt{4N-2} - g_0\sqrt{N}\\ &= g_0\sqrt{N}[\sqrt{4-2/N}-1] \to g_0\sqrt{N} \quad \text{for } N \gg 1.\end{aligned} \tag{2}$$

Of additional note in Fig. 1 are the transition rates and spacings from the upper sideband of the first excited state to levels of the second excited state. As explained in the figure caption, the quantum transitions give rise to an additional ‘‘anharmonic’’ resonance at $(\sqrt{2}-1)g_0$, whereas for $N \gg 1$, the allowed large-N transitions lead to no additional resonances other than at $\pm g_0\sqrt{N}$.

The simple picture presented thus far becomes significantly more complicated under a typical experimental measurement strategy. For example, in our experiment the number of intracavity atoms fluctuates during the detection time window, the coupling is not constant within the cavity mode (it is an optical standing-wave cavity with a Gaussian transverse profile), the system is driven with an external field, and there is dissipation for both the atoms and the cavity.

Unfortunately, a general quantum treatment of the eigenvalue structure of the atom-cavity system for such experimental conditions is a nontrivial undertaking. However, we can nonetheless make some progress in understanding the nature of the eigenstates and eigenvalues for the case of a distribution of atoms in a spatially varying field mode by reference to a simple model. We consider the interaction Hamiltonian $\hat{H}_I$ for N_s atoms in the cavity each with coupling strength $g_l = g(\vec{r}_l)$ at the site $\vec{r}_l$ of the lth atom. Explicitly, in the dipole and rotating-wave approximations we have

$$\hat{H}_I = i\hbar \sum_{l=1}^{N_s} [g_l \hat{a}^\dagger \hat{\sigma}_l^- + g_l^* \hat{a} \hat{\sigma}_l^+], \tag{3}$$

where $\hat{a}$ is the annihilation operator for the cavity field mode and $\hat{\sigma}_l^+$ is the raising operator for the lth atom. To begin with, we restrict our attention to the case of one unit of excitation in the atom-cavity system. Since our interest is in the collective degrees of freedom of the atomic sample, we introduce the state

$$|1\rangle_A \equiv \frac{1}{g_0\sqrt{N_e}} \sum_{l=1}^{N_s} g_l^* |0\rangle_1 |0\rangle_2 \cdots |1\rangle_l \cdots |0\rangle_{N_s}, \tag{4}$$

where $(|0\rangle_j, |1\rangle_j)$ represent the (ground, excited) states of atom j. This state is simply the state of one excitation shared symmetrically among the N_s atoms of the sample. The normalization ${}_A\langle 1|1\rangle_A = 1$ demands that

$$N_e = \frac{1}{g_0^2} \sum_{l=1}^{N_s} |g_l|^2 = \sum_{l=1}^{N_s} |\psi_l|^2, \tag{5}$$

where $\psi(\vec{r}_l) \equiv \psi_l$ is the cavity mode function (defined below). N_e represents the effective number of atoms in the cavity, in which each actual atom is weighted by its coupling to the field mode. Note that for N_s atoms all at optimal sites $(|\psi| = 1)$ $N_e = N_s$.

For the case of one excitation, we introduce the basis states

$$|\psi_1\rangle \equiv |1\rangle_c |0\rangle_A, \quad |\psi_2\rangle \equiv |0\rangle_c |1\rangle_A, \tag{6}$$

where $|n\rangle_c$ is the state of the cavity field with n photons and $|0\rangle_A \equiv |0\rangle_1 |0\rangle_2 \cdots |0\rangle_{N_s}$ is the atomic state with all atoms in the ground state. In this basis, the eigenvalues of the first excited state associated with $\hat{H}_I$ are found to be

$$\lambda_\pm^{(1)} = \pm g_0 \sqrt{N_e}, \tag{7}$$

previously indicated in Fig. 1, now, however, with the replacement $N \rightarrow N_e$.

Turning next to the second excited manifold with two quanta in the atom-cavity system, we introduce the states

$$|\phi_1\rangle \equiv |0\rangle_c |2\rangle_A, \quad |\phi_2\rangle \equiv |1\rangle_c |1\rangle_A, \quad |\phi_3\rangle \equiv |2\rangle_c |0\rangle_A, \tag{8}$$

where now $|2\rangle_A$ is the state with two excitations in the atomic sample (with $N_s > 1$), carried, of course, by distinct atoms. Explicitly we have

$$|2\rangle_A \equiv \frac{1}{\sqrt{D}} \sum_{l \neq p}^{N_s} g_l^* g_p^* |0\rangle_1 \cdots |1\rangle_l \cdots |1\rangle_p \cdots |0\rangle_{N_s}, \tag{9}$$

with normalization

$$D \equiv 2 g_0^4 N_e^2 \left[1 - \frac{\Sigma |\psi_l|^4}{N_e^2} \right]. \tag{10}$$

The eigenvalues of the second excited state for $\hat{H}_I$ follow by diagonalizing the 3×3 matrix in the basis specified by Eq. (8) and are found to be

$$\lambda_0^{(2)} = 0, \quad \lambda_\pm^{(2)} = \pm \sqrt{2} g_0 \sqrt{N_e} \left[2 - \frac{M_e}{N_e^2} \right]^{1/2}, \tag{11}$$

where

$$M_e \equiv \sum_{l=1}^{N_s} |\psi_l|^4. \tag{12}$$

Note that for $N_s = 1$ atom in the sample, at position $\vec{r}_i$, we must have $|2\rangle_A = 0$. In this case, $\langle \phi_2 | \hat{H}_I | \phi_1 \rangle = 0$ and the eigenvalues equation has no $\lambda = 0$ root. Indeed, $\lambda_\pm^{(2)} \rightarrow \sqrt{2} g_0^2 |\psi_i|^2 = \sqrt{2} |g(\vec{r}_i)|^2$ as would be expected from Fig. 1 for one atom with (nonoptimal) coupling g_i.

Returning to the general case $N_s > 1$ for a distributed sample, we compute the transition frequency d_1 (relative to ω_0) for the transition analogous to t_1^* shown in Fig. 1, namely,

$$d_1 = \lambda_+^{(2)} - \lambda_+^{(1)} = g_0 \sqrt{N_e} \left[\sqrt{2} \left(2 - \frac{M_e}{N_e^2} \right)^{1/2} - 1 \right]. \tag{13}$$

In the limit of a sample of N_s atoms in a mode of uniform strength $(|\psi| = 1)$, we have that $M_e \rightarrow N_s$, $N_e \rightarrow N_s$, so that

$$d_1 \rightarrow g_0 \sqrt{N_s} \left[\left(4 - \frac{2}{N_s} \right)^{1/2} - 1 \right], \tag{14}$$

in agreement with Eq. (2). Likewise, the quantum anharmonicity q_a now becomes

$$q_a' \equiv \frac{\lambda_+^{(2)}}{2 g_0 \sqrt{N_s}} = \left(1 - \frac{M_e}{2 N_e^2} \right)^{1/2} \rightarrow q_a \tag{15}$$

for a uniform mode $(|\psi| = 1)$.

It is worth noting that a sample with distributed atoms but with effective atom number $N_e = 1$ gives rise to a larger splitting for the second excited state than does a single atom, $N_s = 1$. The reason for this can be understood with reference to Eqs. (8) and (9), and in particular to the contribution from the state $|2\rangle_A$. The classical limit requires $\lambda_+^{(2)} \rightarrow 2\sqrt{N_e} g_0$, which is larger than the quantum (single-atom) result $\sqrt{2} g_0$.

It is precisely the ''classical'' contribution from excitations of two separate atoms in Eq. (9) [$\mathcal{O}(N_s^2)$ such terms] that overwhelm the ''quantum'' contribution from the state $|\phi_2\rangle$ in Eq. (8) [$\mathcal{O}(N_s)$ such terms]. That is, if we by *fiat* drop the contribution associated with the two excited atoms in the sample (the state $|\phi_1\rangle$), we then find the eigenvalues for the second excited state to be

$$\Lambda_{\pm}^{(2)}=\pm\sqrt{2N_e}g_0, \tag{16}$$

such that

$$l_1\equiv\Lambda_{+}^{(2)}-\lambda_{+}^{(1)}=g_0\sqrt{N_e}(\sqrt{2}-1). \tag{17}$$

Note that the quantum anharmonicity remains. Hence $\lambda_{+}^{(2)}$ for the case of a distributed sample lies between this quantum result $\sqrt{2N_e}g_0$ and the classical result $2\sqrt{N_e}g_0$, approaching the latter for $N_e\gg 1$.

Not surprisingly, the quantitative values for $\lambda_{\pm}^{(2)}$ depend on the particular locations of atoms within the mode volume. For an atomic beam experiment such as ours, we can think of repeated trials associated with different realizations of atoms at various sites within the mode volume, where independent trials are roughly realized in a time scale associated with atomic transit through the cavity mode. In such a case, both N_s and the quantities (N_e, M_e) will vary from one realization to the next, with the constraint that the average atomic density be constant. Hence the quantities (N_e, M_e) appearing in Eq. (11) for $\lambda_{\pm}^{(2)}$ will vary from realization to realization. Here we anticipate the results of Sec. III where Monte Carlo simulations are performed and from which the average value $\langle d_1\rangle$ can be obtained, where

$$\langle d_1\rangle=\left\langle g_0\sqrt{\sum_i|\psi_i|^2}\left[\sqrt{2}\left(2-\frac{\Sigma_j|\psi_j|^4}{(\Sigma_l|\psi_l|^2)^2}\right)^{1/2}-1\right]\right\rangle, \tag{18}$$

with the angular brackets representing an average over repeated trials of randomly generated atomic positions. We consider a Gaussian standing-wave mode with

$$\psi(\vec{r})=\sin(kz)\exp[-(x^2+y^2)/w_0^2]. \tag{19}$$

Collecting together the results thus far obtained, we present in Fig. 2 a plot of the quantities $(\delta_1,\ l_1,\langle d_1\rangle)$ where we recall that these are the transition frequencies (relative to ω_0) from the upper state of the first excited level to the upper state of the second excited level with δ_1 being the frequency for a sample of atoms in a uniform mode ($|\psi|=1$) (or at a fixed point in a spatially varying mode), l_1 being the corresponding ''quantum'' component obtained by excluding the two single-atom excitations of the state $|\phi_1\rangle$, and $\langle d_1\rangle$ being the Monte Carlo average as in Eq. (18) obtained for a Gaussian standing-wave cavity.

We also include in Fig. 2 the analytic result for a continuous sample of uniform density ρ (our ''jelly'' model), for which

$$N_e\equiv\sum_i|\psi_i|^2\rightarrow\rho\int|\psi(\vec{r})|^2d^3x\equiv\rho V_0, \tag{20}$$

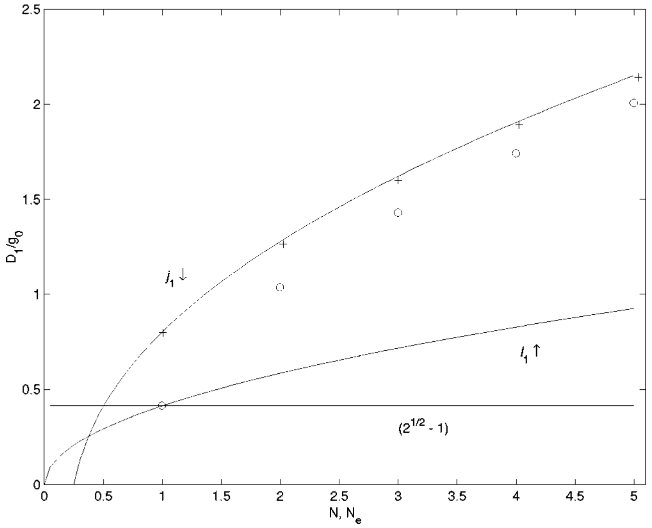

FIG. 2. Frequency D_1/g_0 for the transition from the upper state of the first excited manifold to the upper state of the second excited manifold (t_1^* in Fig. 1) vs number of atoms, either N_e (a continuous variable) for distributed samples or N (an integer variable) for fixed, optimally coupled samples. Here D_1 is one of the four quantities $\{\delta_1,l_1,\langle d_1\rangle,j_1\}$ defined in Eqs. (2), (17), (18), and (24). The + are points from the numerical simulation $\langle d_1\rangle$ for a Gaussian standing-wave cavity mode, and the ○ are δ_1, the fixed, optimally coupled case.

with

$$V_0\equiv\int|\psi(\vec{r})|^2d^3x=\frac{\pi w_0^2 l}{4} \tag{21}$$

as the effective mode volume. We again specialize to the case of a standing-wave Gaussian mode cavity with a sample of infinite extent along the (x,y) plane and distributed along the length l of the cavity axis. Likewise,

$$M_e\equiv\sum_i|\psi_i|^4\rightarrow\rho\int|\psi(\vec{r})|^4d^3x\equiv\frac{3}{8}\rho V_0, \tag{22}$$

so that

$$k\equiv M_e/N_e=\frac{3}{8}. \tag{23}$$

For the Gaussian standing-wave cavity with a continuous sample of density ρ (as opposed to one composed of discrete atoms situated throughout the mode), we thus find from Eqs. (23) and (13) that

$$d_1\rightarrow j_1=g_0\sqrt{N_e}\left[\sqrt{2}\left(2-\frac{3}{8N_e}\right)^{1/2}-1\right] \tag{24}$$

for the transition frequency of the upper to upper states of the first and second excited manifolds. Note that the analytic form for j_1 [Eq. (24)] gives a reasonable approximation to the expectation value of Eq. (18).

B. Heisenberg equations of motion

While the underlying quantum structure of the coupled atom-cavity system in the absence of drive or dissipation is well understood, probing that structure in the laboratory has proved a challenging task. A number of measurement strategies have been theoretically investigated, including single-field coherent excitation [37,42,43] and excitation with incoherent light [42,44,45]. Unfortunately, all of these analyses are for a single atom located at a fixed site $\vec{r}_0$ inside the cavity mode. It seems clear that a general treatment of the eigenvalue structure of the atom-cavity system in the presence of continuous excitation and dissipation is a nontrivial theoretical undertaking. Beyond the extension of the plane-wave theory of the preceding section to the case of N_s atoms each with a different coupling to the cavity, our experiment involves as well fluctuations in atomic number and position and the system is driven, so that the situation becomes more complicated still. In general there are drive strength-dependent level shifts [37] and the intracavity field buildup depends on the exact number and position of the collection of atoms. In response to our experimental investigation, Tian and Carmichael [46] have explored a pump-probe-type measurement and developed both a semiclassical and fully quantum theoretical treatment of the nonlinear transmission spectrum of the coupled atom-cavity system, including atomic beam effects; their complete quantum Monte Carlo simulation is rather bulky, and so the details will not be discussed here. Additionally, Tian and Carmichael have developed a different approach which utilizes a photon coincidence detection scheme to extract the interesting nonlinear features of the Jaynes-Cummings model [32,33] from an atomic beam experiment. The calculations for this scheme are quite reasonable in required resources and demonstrate that the experimental scheme is very promising. Here we will not present a full discussion of all measurement strategies available, but instead we will focus on the spectra measurements within which context we will pursue several calculational approaches, each with a limited domain of validity.

In particular, in this section we begin with the Heisenberg equations of motion for the cavity field $\hat{a}$, the atomic polarization $\hat{\sigma}_l^-$, and inversion $\hat{\sigma}_l^z$ for the lth atom at site $\vec{r}_l$ in a sample of N_s atoms. We follow a standard procedure [39] by way of a quantum master equation for the density operator $\hat{\rho}$ to obtain the following Heisenberg equations of motion for the N_s two-state atoms interacting via $\hat{H}_I$ of Eq. (3) with a single spatially varying field mode:

$$\dot{\hat{a}} = -(\kappa + i\Theta)\hat{a} + \sum_{l=1}^{N_s} g(\vec{r}_l)\hat{\sigma}_l^- + \varepsilon, \tag{25}$$

$$\dot{\hat{\sigma}}_l^- = -(\gamma_\perp + i\Delta)\hat{\sigma}_l^- + g(\vec{r}_l)\hat{a}\hat{\sigma}_l^z, \tag{26}$$

$$\dot{\hat{\sigma}}_l^z = -\gamma_\parallel(\hat{\sigma}_l^z + 1) - 2g(\vec{r}_l)(\hat{a}^\dagger\hat{\sigma}_l^- + \hat{a}\hat{\sigma}_l^+). \tag{27}$$

Here ε denotes a coherent driving field at frequency ω_p [which defines the rotating frame for Eqs. (25)–(27)], $\Theta = (\omega_c - \omega_p)/\kappa$ is the cavity detuning, $\Delta = (\omega_a - \omega_p)/\gamma_\parallel$ is the atomic detuning, κ is the cavity field decay rate, and $\gamma_\perp$ is the transverse atomic decay. For pure radiative decay $\gamma_\perp = \gamma_\parallel/2$. Note that $\gamma_\parallel$ is in general the decay rate to modes other than the privileged cavity mode. However, for our cavities, $\gamma_\parallel$ is essentially the same as for an atom in free space since we operate in the limit that the solid angle (f) subtended by the cavity mode is small ($f \approx 10^{-5}$). Finally, the dipole coupling coefficient for an atom with transition moment μ at site $\vec{r}$ within the cavity standing wave is $g(\vec{r}) \equiv g_0\psi(\vec{r})$, where $g_0 \equiv (\mu^2\omega_c/2\hbar\epsilon_0 V)^{1/2}$ is the optimal coupling coefficient and $\psi(\vec{r}) \equiv \sin(kz)\exp[-(x^2+y^2)/\omega_0^2]$ is the cavity mode function for our Gaussian standing-wave mode with mode volume $V_m \equiv \int_{-\infty}^{\infty}dx\int_{-\infty}^{\infty}dy\int_0^l dz|\psi(x,y,z)|^2 = \pi\omega_0^2 l/4$. Two useful dimensionless quantities which can be derived from the rates (κ,γ,g) are the saturation photon number $n_s \equiv b\gamma_\perp\gamma_\parallel/4g^2$, where $b = 8/3$ for a Gaussian standing-wave mode [47], and the critical atom number $N_0 \equiv 2\gamma_\perp\kappa/g_0^2$. Our task now is to understand the behavior predicted by Eqs. (25)–(27) for various drive configurations and strengths.

It is of course the terms $\hat{a}\hat{\sigma}_l^z$ and $\hat{a}\hat{\sigma}_l^-$ (and conjugate terms) which couple Eqs. (25)–(27) to an infinite hierarchy of equations for higher-order products of atom and field operators and which make the general atom-cavity problem difficult to solve in its full generality. However, in the limit of vanishing excitation, we can restrict our attention to a limited basis set consisting of only three direct product states. The first state is the ground state $|\psi_0\rangle = |0\rangle_A|0\rangle_c$ with no excitation in atoms or field; the second state places one excitation in the cavity mode with all atoms in their ground states and is just the state $|\psi_1\rangle$ of Eq. (6); the third state contains one excitation distributed among the atoms with the field in its ground state and is the state $|\psi_2\rangle$ of Eq. (6). Taking expectation values in this restricted basis, we find that the product $\langle\hat{a}\hat{\sigma}_l^z\rangle = (-1)\langle\hat{a}\rangle$ and hence

$$\langle\dot{\hat{\sigma}}_l^-\rangle = -(\gamma_\perp + i\Delta)\langle\hat{\sigma}_l^-\rangle - g(\vec{r}_l)\langle\hat{a}\rangle. \tag{28}$$

For $\varepsilon = 0$, Eq. (25) (its expectation value) and Eq. (28) form a coupled homogeneous system for $N_s + 1$ complex variables whose eigenvalues are straightforward to deduce. The "atomic" eigenvalue $\lambda_A = -(\gamma_\perp + i\Delta)$ is $(N_s - 1)$-fold degenerate, while the remaining two eigenvalues $\lambda_\pm$ are found as roots of the quadratic

$$f(\lambda) \equiv [\lambda + (\kappa + i\Theta)][\lambda + (\gamma_\perp + i\Delta)] + g_0^2 N_e, \tag{29}$$

where in agreement with our earlier definition [Eq. (5)] $N_e = \Sigma_{l=1}^{N_s}|\psi_l|^2$. Also, for $\kappa = 0 = \gamma_\perp$ (in the absence of dissipation), the eigenvalues given by Eq. (29) reproduce the result of Eq. (7), namely,

$$\lambda_\pm^{(1)} = \pm g_0\sqrt{N_e}. \tag{30}$$

Note that the $N_s - 1$ eigenvectors corresponding to λ_A are such that $\Sigma_l g_l\langle\hat{\sigma}_l^-\rangle = 0$ and $\langle\hat{a}\rangle = 0$ which represents no excitation of the "collective" or "cooperative" degrees of freedom. On the other hand, the eigenvectors corresponding to $\lambda_\pm$ describe the dynamics of the collective atom-cavity system. As indicated in Eq. (25), this collective degree of freedom can be explored by way of excitation of the cavity field $\hat{a}$, which couples to each atom in precisely the manner specified by the expansion in Eq. (4) (namely, in direct proportion to g_l) and is driven by the collective response of all atoms.

More specifically, consider conditions of weak excitation ($\varepsilon/\kappa \ll 1$) such that the three-state basis $\{|\psi_0\rangle, |\psi_1\rangle, |\psi_2\rangle\}$ suffices. In this case, Eqs. (25) and (28) are readily solved in steady state. The transmission function $t_{\mathrm{lin}}(\omega_p)$ of a weak external probe, operationally defined as the ratio of transmitted to incident field amplitude, is, in the case of coincident cavity and atomic frequencies ($\omega_c = \omega_a$), given by [25,48]

$$t_{\mathrm{lin}}(\omega_p) = \frac{\kappa[\gamma_\perp - i\omega_p]}{(\lambda_+ - i\omega_p)(\lambda_- - i\omega_p)}. \tag{31}$$

The eigenvalues $\lambda_\pm$ are given by

$$\lambda_\pm = -\left(\frac{\kappa+\gamma_\perp}{2}\right) \pm \left[\left(\frac{\kappa-\gamma_\perp}{2}\right) - g_0^2 N_e\right]^{1/2}, \tag{32}$$

and describe the collective normal modes of the coupled system. Note that in the weak-field limit considered here, $\lambda_\pm$ simply contain $g_0\sqrt{N_e}$ to account for the varied couplings of the N_s atoms. Equations (31) and (32) are valid as long as the excitation is ''weak'' ($\epsilon/\kappa \to 0$) so that our assumed basis $|\psi_{0,1,2}\rangle$ is adequate. This is simply the case of coupled linear oscillators. That is to say, either the approach we have adopted here or an approach utilizing the full quantum master equation leads to the same prediction of normal-mode structure [Eq. (32)] and the same transmission function [Eq. (31)].

From Eq. (32), a normal-mode splitting is formally expected for $g_0\sqrt{N_e} > (\gamma_\perp - \kappa)/2$ with corresponding $\lambda_\pm \approx -(\kappa+\gamma_\perp)/2 \pm i g_0\sqrt{N_e}$. Only if $g_0\sqrt{N_e} > (\kappa+\gamma_\perp)/2$ will the splitting be observable. Considering the observability of the normal-mode splitting for the case $N_e = 1$ we adopt the criterion $g_0 > (\kappa, \gamma_\perp)$ for the strong-coupling regime. The imaginary parts of the resulting eigenvalues give rise to a normal-mode splitting, which in the case $N_e = 1$ (in the optimal coupling limit), is known equivalently as the single-atom vacuum-Rabi splitting at $\pm g_0$ or the first excited state of the Jaynes-Cummings ladder, as was first observed in direct spectroscopic measurements [1,17,20] in our group.

C. Semiclassical theory

As has been demonstrated repeatedly over the past 15 years, the utility of a semiclassical model of the coupled atom-cavity system is far-reaching. In addition, the semiclassical equations are tractable from the perspective of modeling a real experiment in which fluctuations, dissipation and drive must be treated.

We thus turn next to a semiclassical treatment. The well-known Maxwell-Bloch equations for the expectation value of the cavity field mode $\langle\hat{a}\rangle$, the atomic polarization $\langle\hat{\sigma}_l^-\rangle$, and inversion $\langle\hat{\sigma}_l^z\rangle$ for the lth atom in a sample of N_s atoms are arrived at from the full quantum equations (25)–(27) by the simple replacements

$$\langle\hat{\sigma}_l^z\hat{a}\rangle \to \langle\hat{\sigma}_l^z\rangle\langle\hat{a}\rangle, \quad \langle\hat{a}^\dagger\hat{\sigma}_l^+\rangle \to \langle\hat{a}^\dagger\rangle\langle\hat{\sigma}_l^z\rangle,$$
$$\langle\hat{a}\hat{\sigma}_l^-\rangle \to \langle\hat{a}\rangle\langle\hat{\sigma}_l^-\rangle, \tag{33}$$

and read

$$\langle\dot{\hat{a}}\rangle = -(\kappa + i\Theta)\langle a\rangle + \sum_l^{N_s} g(\vec{r}_l)\langle\hat{\sigma}_l^-\rangle + \varepsilon, \tag{34}$$

$$\langle\dot{\hat{\sigma}}_l^-\rangle = -(\gamma_\perp + i\Delta)\langle\hat{\sigma}_l^-\rangle + g(\vec{r}_l)\langle\hat{a}\rangle\langle\hat{\sigma}_l^z\rangle, \tag{35}$$

$$\langle\dot{\hat{\sigma}}_l^z\rangle = -\gamma_\parallel(\langle\hat{\sigma}_l^z\rangle + 1) - 2g^*(\vec{r}_l)(\langle\hat{a}^\dagger\rangle\langle\hat{\sigma}_l^-\rangle + \langle\hat{a}\rangle\langle\hat{\sigma}_l^+\rangle). \tag{36}$$

Note that in the limit of weak excitation $\varepsilon \to 0$ such that $\langle\hat{a}\rangle \ll \sqrt{n_s}$, the eigenvalues which follow from Eqs. (34)–(36) are precisely those of the full quantum theory [Eqs. (29) and (32)]. Further, the transmission function for the probe field is just that of Eq. (31). There is no surprise here, in either the quantum or classical case; for weak excitation, we are simply probing the normal-mode structure for the two coupled (linear) oscillators associated with the collective atomic polarization and the intracavity field.

Of considerable more current interest [28] is an exploration of the structure of the higher-lying states shown in Fig. 1 as was discussed in Sec. II A. However, as we previously noted, the formulation of a full quantum theory for our experiment is a somewhat daunting undertaking. We will instead settle for a preliminary attack on this problem by way of the semiclassical equations (34)–(36), which are much more amenable to extensions which include fluctuations in atomic number and position.

Our semiclassical theory is developed to correspond to our experimental strategy which is to first excite one of the two ''levels'' of the first excited manifold shown in Fig. 1 with a fixed frequency ''pump'' field ϵ_p. A second ''probe'' beam of tunable frequency can then excite transitions from the first to the second manifold of excited states, and thereby reveal the structure of the dressed states containing two excitations. Excitation of the *field* mode probes this structure in the same way discussed above for the first excited state.

In formal terms, we supplement Eq. (34) with a probe field of amplitude ϵ' and frequency ν by the replacement

$$\varepsilon \to \epsilon_p + \epsilon' e^{-i\nu t}, \tag{37}$$

where ϵ_p represents the pump field [recall that Eqs. (34)–(36) are written in a rotating frame, here taken at ω_{pump}, the frequency of the pump field]. Thus ν is the offset frequency of the probe relative to the pump. We treat ϵ' as a perturbation (as compared to the steady state established by ϵ_p), and write

$$\alpha(t) = \alpha^{ss} + \delta\alpha(t), \quad p_l(t) = p_l^{ss} + \delta p_l(t),$$
$$z_l(t) = z_l^{ss} + \delta z_l(t), \tag{38}$$

where $\alpha \equiv \langle\hat{a}\rangle$, $p_l \equiv \langle\hat{\sigma}_l^-\rangle$, $z_l \equiv \langle\hat{\sigma}_l^z\rangle$, and ss denotes the steady-state solution established with the pump field alone

$(\epsilon'=0,\epsilon_p\neq 0)$. Substituting Eqs. (38) into Eqs. (34)–(36) with Eq. (37) yields the following equations for the deviations $(\delta\alpha,\delta p_l,\delta z_l)$:

$$\delta\dot{\alpha}(t)=-(\kappa+i\Theta)\delta\alpha(t)+\sum g_l\delta+\epsilon' e^{-i\nu t}\quad\text{and c.c,}\tag{39}$$

$$\delta\dot{p}_l(t)=-(\gamma_\perp+i\Delta)\delta p_l(t)+g_l^*[\alpha_{ss}\delta z_l+z_l^{ss}\delta\alpha]\quad\text{and c.c.,}\tag{40}$$

$$\begin{aligned}\delta\dot{z}_l(t)=&-\gamma_\parallel\delta z_l(t)-2g_l[\alpha_{ss}^*\delta p_l+p_l^{ss}\delta\alpha^*]\\&-2g_l^*[\alpha_{ss}\delta p_l^*+(p_l^{ss})^*\delta\alpha].\end{aligned}\tag{41}$$

Introducing the Fourier transform of each variable, e.g.,

$$\widetilde{z}(\Omega)\equiv\int e^{i\Omega t}\delta z(t)dt,\tag{42}$$

we find

$$\begin{aligned}0=&-(\kappa+i\Theta-i\Omega)\widetilde{\alpha}(\Omega)+\sum_l g_l\widetilde{p}_l(\Omega)\\&+2\pi\epsilon'\delta(\Omega-\nu),\end{aligned}$$

$$\begin{aligned}0=&-(\kappa-i\Theta-i\Omega)\widetilde{\alpha}^*(\Omega)+\sum_l g_l^*\widetilde{p}_l^*(\Omega)\\&+2\pi\epsilon^{*\prime}\delta(\Omega+\nu),\end{aligned}\tag{43}$$

$$0=-(\gamma_\perp+i\Delta-i\Omega)\widetilde{p}_l(\Omega)+g_l^*[\alpha_{ss}\widetilde{z}_l(\Omega)+z_l^{ss}\widetilde{\alpha}(\Omega)],$$

$$\begin{aligned}0=&-(\gamma_\perp-i\Delta-i\Omega)\widetilde{p}_l^*(\Omega)\\&+g_l[\alpha_{ss}^*\widetilde{z}_l(\Omega)+z_l^{ss}\widetilde{\alpha}^*(-\Omega)],\end{aligned}\tag{44}$$

$$\begin{aligned}0=&-(\gamma_\parallel-i\Omega)\widetilde{z}_l(\Omega)-2g_l[\alpha_{ss}^*\widetilde{z}_l(\Omega)+z_l^{ss}\widetilde{\alpha}^*(-\Omega)],\\&-2g_l^*[\alpha_{ss}\widetilde{z}_l(\Omega)+z_l^{ss}\widetilde{\alpha}(\Omega)].\end{aligned}\tag{45}$$

Equations (44) and (45) can be combined to find an expression for $\widetilde{p}_l(\Omega)$ in terms of the steady-state solutions $(\alpha_{ss},p_l^{ss},z_l^{ss})$ and $\widetilde{\alpha}(\Omega)$, namely,

$$\begin{aligned}\widetilde{p}_l(\Omega)=&\frac{g_l^*}{(\gamma_\perp+i\Delta-i\Omega)}\left\{\left[(\gamma_\parallel-i\Omega)+2|g_l|^2\left(\frac{|\alpha_{ss}|^2}{(\gamma_\perp+i\Delta-i\Omega)}+\frac{|\alpha_{ss}|^2}{(\gamma_\perp-i\Delta-i\Omega)}\right)\right]^{-1}\right.\\&\left.\times\left[-2z_l^{ss}|g_l|^2\left(\frac{|\alpha_{ss}|^2\widetilde{\alpha}(\Omega)}{(\gamma_\perp+i\Delta-i\Omega)}+\frac{|\alpha_{ss}|^2\widetilde{\alpha}^*(-\Omega)}{(\gamma_\perp-i\Delta-i\Omega)}\right)-2g_lp_l^{ss}\alpha_{ss}\widetilde{\alpha}^*(-\Omega)-2g_l^*(p_l^{ss})^*\alpha_{ss}\widetilde{\alpha}(\Omega)\right]+z_l^{ss}\widetilde{\alpha}(\Omega)\right\}.\end{aligned}\tag{46}$$

At this point, we turn to evaluate explicitly the steady-state quantities $(\alpha_{ss},p_l^{ss},z_l^{ss})$ required in this expression. Since the situation follows along the well-worn path of the optical bistability literature [25], we simply quote the results:

$$z_l^{ss}=\frac{-(1+\delta^2)}{1+\delta^2+|\alpha_{ss}|^2/n_0^l},\qquad p_l^{ss}=\frac{\frac{-g_l^*}{\gamma_\perp}\alpha}{1+i\delta}\left[\frac{1+\delta^2}{1+\delta^2+|\alpha_{ss}|^2/n_0^l}\right],\tag{47}$$

$$\begin{aligned}\frac{\epsilon_p}{\kappa}=\alpha_{ss}\Bigg[&\left(1+\sum_{l=1}^{N_s}\frac{2C_l}{1+\delta^2+|\alpha_{ss}|^2/n_0^l}\right)\\&+i\left(\phi-\sum_{l=1}^{N_s}\frac{2C_l\delta}{1+\delta^2+|\alpha_{ss}|^2/n_0^l}\right)\Bigg].\end{aligned}$$

Here $n_0^l\equiv\gamma_\perp\gamma_\parallel/(4|g_l|^2)$ and $C_l\equiv|g_l|^2/(2\kappa\gamma_\perp)$ are the saturation photon number and the cooperativity parameter for an atom at site $\vec{r}_l$ [49]. The normalized atomic and cavity detunings are defined by $\delta\equiv\Delta/\gamma_\perp$ and $\phi\equiv\Theta/\kappa$.

Our objective here is to find a simple analytic form for the transmission of the probe field ϵ' as a function of ν in the presence of the pump field ϵ_p. With such an expression, we can then efficiently perform Monte Carlo averages over randomly generated distributions of atomic positions to simulate our atomic beam experiment. Towards this end, we seek an expression valid to lowest order in $|\alpha_{ss}|^2$ and hence expand the various quantities in Eqs. (47) as follows:

$$z_l^{ss}\approx-\left[1-\frac{|\alpha_{ss}|^2}{n_0^2(1+\delta^2)}\right],\tag{48}$$

$$\begin{aligned}p_l^{ss}\approx&\frac{-g_l^*}{\gamma_\perp}(1-i\delta)\alpha_{ss}\left[1-\frac{|\alpha_{ss}|^2}{n_0^2(1+\delta^2)}\right]\\\equiv&\, p_l^0\left[1-\frac{|\alpha_{ss}|^2}{n_0^2(1+\delta^2)}\right],\end{aligned}\tag{49}$$

$$\left|\frac{\epsilon_p}{\kappa}\right|^2 \approx |\alpha_{ss}|^2 \left[\left(1 + \frac{2C_1 N_e}{1+\delta^2} - \frac{2C_1|\alpha_{ss}|^2}{(1+\delta^2)m_0} M_e \right)^2 + \left(\phi - \frac{2C_1 N_e \delta}{1+\delta^2} + \frac{2C_1|\alpha_{ss}|^2 \delta}{(1+\delta^2)m_0} M_e \right)^2 \right], \tag{50}$$

where we define the optimal saturation photon number and single-atom cooperativity as $m_0 \equiv \gamma_\perp \gamma_\parallel/(4g_0^2)$ and $C_1 \equiv g_0^2/(2\kappa\gamma_\perp)$, respectively.

Combining Eqs. (46) and (48), (49) and retaining only lowest-order terms in $|\alpha_{ss}|$, we find

$$\widetilde{p}_l(\Omega) = \frac{g_l^*}{\gamma_\perp + i\Delta - i\Omega} \left[-\widetilde{\alpha}(\Omega) \left(1 - \frac{|\alpha_{ss}|^2}{(1+\delta^2)n_0^l} \right) + \frac{2|g_l|^2}{(\gamma_\parallel - i\Omega)} |\alpha_{ss}|^2 \widetilde{\alpha}(\Omega) \left[\frac{2\gamma_\perp - i\Omega}{(\gamma_\perp - i\Delta)(\gamma_\perp + i\Delta - i\Omega)} \right] + \frac{2|g_l|^2}{(\gamma_\parallel - i\Omega)} \times \alpha_{ss}^2 \widetilde{\alpha}^*(-\Omega) \left(\frac{2\gamma_\perp - i\Omega}{(\gamma_\perp + i\Delta)(\gamma_\perp - i\Delta - i\Omega)} \right) \right]. \tag{51}$$

By forming the sum $\Sigma g_l \widetilde{p}_l(\Omega)$ with Eq. (51), we can eliminate the dipole source term in Eq. (43) to be left with

$$\widetilde{\alpha}(\Omega)(\kappa + i\Theta - i\Omega) = \frac{N_e g_0^2 \widetilde{\alpha}(\Omega)}{(\gamma_\perp + i\Delta - i\Omega)} + \frac{2M_e g_0^4 (2\gamma_\perp - i\Omega)|\alpha_{ss}|^2 \widetilde{\alpha}(\Omega)}{(\gamma_\parallel - i\Omega)(\gamma_\perp - i\Delta)(\gamma_\perp + i\Delta - i\Omega)^2} + \frac{2M_e g_0^4 (2\gamma_\perp/\gamma_\parallel)|\alpha_{ss}|^2 \widetilde{\alpha}(\Omega)}{(\gamma_\perp^2 + \Delta^2)(\gamma_\perp + i\Delta - i\Omega)} + \frac{2M_e g_0^4 (2\gamma_\perp - i\Omega)\alpha_{ss}^2 \widetilde{\alpha}^*(-\Omega)}{(\gamma_\parallel - i\Omega)(\gamma_\perp + i\Delta)(\gamma_\perp - i\Delta - i\Omega)(\gamma_\perp + i\Delta - i\Omega)} + 2\pi\epsilon' \delta(\Omega - \nu), \tag{52}$$

where in correspondence to Eqs. (5) and (11) we have defined $N_e \equiv \Sigma_l |\psi_l|^2$ and $M_e \equiv \Sigma_l |\psi_l|^4$. Notice now that by writing a corresponding equation for $\widetilde{\alpha}^*(-\Omega)$ the term in $\delta(\Omega - \nu)$ will not contribute to heterodyne detection at the probe frequency ν as in our experiment. Without this term, then, the resulting equation for $\widetilde{\alpha}^*(-\Omega)$ is given in terms of $\widetilde{\alpha}(\Omega)$ with a lowest-order contribution $|\alpha_{ss}|^4$. Hence, to order $|\alpha_{ss}|^2$, we can drop the $\widetilde{\alpha}^*(-\Omega)$ term in Eq. (52) altogether to find

$$\widetilde{\alpha}(\Omega) = 2\pi \frac{\epsilon'}{\kappa} \delta(\Omega - \nu) t_p(\Omega) \times \left[1 - \frac{2|\alpha_{ss}|^2 g_0^4 M_e t_p(\Omega)}{\kappa(\gamma_\perp + i\Delta - i\Omega)} \left(\frac{2\gamma_\perp/\gamma_\parallel}{(\gamma_\perp^2 + \Delta^2)} + \frac{(2\gamma_\perp - i\Omega)}{(\gamma_\parallel - i\Omega)(\gamma_\perp - i\Delta)(\gamma_\perp + i\Delta - i\Omega)} \right) \right]^{-1}, \tag{53}$$

where the probe transmission spectrum in the weak-field limit ($|\alpha|^2 \rightarrow 0$) is defined by

$$t_p(\Omega) \equiv \frac{\kappa(\gamma_\perp + i\Delta - i\Omega)}{(\kappa + i\Theta - i\Omega)(\gamma_\perp + i\Delta - i\Omega) + g_0^2 N_e}. \tag{54}$$

Note that Ω in this expression is defined relative to the pump frequency ω_{pump}, which will in fact be varied to one of several values in our experiment. It is somewhat more convenient to translate to a frequency scale centered on the atomic resonance ω_A. Hence we define

$$\Omega \rightarrow \Omega' = \Omega - (\omega_A - \omega_{\text{pump}}) = \Omega - \Delta, \quad \nu \rightarrow \nu' = \nu - \Delta, \tag{55}$$

and rewrite the above expressions as

$$\widetilde{\alpha}(\Omega') = 2\pi \frac{\epsilon'}{\kappa} \delta(\Omega' - \nu') t_p(\Omega) \times \left[1 - \frac{2|\alpha_{ss}|^2 g_0^4 M_e t_p(\Omega')}{\kappa(\gamma_\perp - i\Omega')} \left(\frac{2\gamma_\perp/\gamma_\parallel}{(\gamma_\perp^2 + \Delta^2)} + \frac{2\gamma_\perp - i(\Omega' + \Delta)}{[\gamma_\parallel - i(\Omega' + \Delta)](\gamma_\perp - i\Delta)(\gamma_\perp - i\Omega')} \right) \right]^{-1}, \tag{56}$$

where now

$$t_p(\Omega') \equiv \frac{\kappa(\gamma_\perp - i\Omega')}{\{\kappa + i[(\omega_c - \omega_A) - \Omega']\}(\gamma_\perp - i\Omega') + g_0^2 N_e}. \tag{57}$$

To find the probe transmission spectrum for a given (fixed) input field ϵ we must first deduce $|\alpha_{ss}|^2$ from Eq. (50). Apart from the various detunings and coupling parameters (C_1, n_0) this determination requires an evaluation of the mode sums $N_e \equiv \Sigma |\psi_l|^2$ and $M_e \equiv \Sigma |\psi_l|^4$ for the particular distribution of atoms at hand and, hence, the solution of the cubic equation (50). With $|\alpha_{ss}|^2$ in hand, $\widetilde{\alpha}(\Omega)$ follows in a straightforward fashion from Eq. (56), again with (N_e, M_e) for the particular atom distribution within the cavity mode.

We can recast Eqs. (55), (56), (57), and (50) in a form more similar to that of Eq. (31) and in a terminology more directly related to experimental quantities. As such, the transmission spectrum of a weak probe at a frequency ω (also detected at ω) in the presence of the pump field is

$$t_{\mathrm{nonlin}}(\omega,N_e,M_e)=t_p(\omega,N_e)[1-n_{\mathrm{u}}t_p(\omega,N_e)h_p(\omega,M_e)]^{-1}, \tag{58}$$

where $n_{\mathrm{u}}\equiv|\alpha_{ss}|^2$ is the pump intracavity photon number and

$$h_p(\omega,M_e)=\frac{2g_0^4M_e}{\kappa(\gamma_\perp-i\omega)}\left[\frac{2\gamma_\perp}{\gamma_\parallel(\gamma_\perp^2+\Delta_{\mathrm{u}}^2)}+\frac{2\gamma_\perp-i\omega-i\Delta_{\mathrm{u}}}{(\gamma_\parallel-i\omega-i\Delta_{\mathrm{u}})(\gamma_\perp-i\Delta_{\mathrm{u}})(\gamma_\perp-i\omega)}\right], \tag{59}$$

with Δ_{u} the detuning between the pump frequency and the uncoupled, coincident atom and cavity frequencies.

The linear transmission part $t_p(\omega,N_e)$ appearing in Eq. (58) is given by

$$t_p(\omega,N_e)=\frac{\kappa(\gamma_\perp-i\omega)}{(\kappa-i\omega)(\gamma_\perp-i\omega)+g_0^2N_e}, \tag{60}$$

which is just a rewritten version of Eq. (31). We have allowed $2\gamma_\perp/\gamma_\parallel\neq1$ to account for a slight transit broadening (see Refs. [50] and [29] for a discussion of the validity of this approximation). Equations (58)–(60) are a complete specification of the transmission of a weak probe in the presence of a pump field with intracavity photon number n_{u} and detuning Δ_{u} for an atom-cavity system with effective atom number N_e and moment M_e.

In a Monte Carlo numerical simulation of the experiment, we do not know the intracavity pump photon number *a priori* since we drive the atom cavity with a fixed-power, fixed-frequency *external* pump field, of strength i_{in}. To reiterate the previous discussion, for each distribution (each instance of N_e,M_e), the pump intracavity photon number n_{u} is found by inverting the following equation:

$$i_{\mathrm{in}}=n_{\mathrm{u}}\left[\left(1+\frac{2C_1N_e}{1+d^2}-\frac{2C_1n_{\mathrm{u}}M_e}{n_0(1+d^2)^2}\right)^2+\left(\phi-\frac{2C_1N_ed}{1+d^2}-\frac{2C_1n_{\mathrm{u}}M_ed}{n_0(1+d^2)^2}\right)^2\right], \tag{61}$$

where $d=\Delta_{\mathrm{u}}/\gamma_\perp$ and $\phi=\Delta_{\mathrm{u}}/\kappa$. So, in total, with Eqs. (58)–(61), we now have a complete description of the probe transmission for a fixed external drive which can be related to an experimental measurement.

Since Eq. (56) is deduced in lowest order in $|\alpha_{ss}|^2$, the pump field cannot be ''too large.'' To quantify this statement, we have compared our approximate result with that of Tian and Carmichael [46] whose analysis is restricted to a single atom at a well-defined site $\vec{r}_0$, but which is valid for arbitrary pump strength. For parameters comparable to those of our experiment, the resulting probe spectra or, more precisely, the difference spectra defined by

$$D_p(\Omega)\equiv|\tilde{\alpha}(\Omega)|^2-|t_p(\Omega)|^2 \tag{62}$$

are essentially indistinguishable for intracavity photon number $|\alpha_{ss}|^2=0.01$ with deviations of about 10% for $|\alpha_{ss}|^2=0.06$ in a situation where the saturation photon number $m_0=0.06$ $[(g,\kappa,\gamma_\parallel=2\gamma_\perp)=(7.2,0.7,5.0)$ MHz]. Since our expansion in $|\alpha_{ss}|^2$ is essentially in terms of the small parameter $|\alpha_{ss}|^2/m_0$, this expansion for the $N=1$ atom case should be sufficient for the more general case of a distributed sample of atoms, as long as $|\alpha_{ss}|^2/m_0<1$ and the modifications of the weak-field spectrum by the pump field are not too large ($\lesssim10\%$).

As implied above, we expect the semiclassical treatment to make incorrect structural predictions as $N_e\rightarrow1$ in the strong-coupling regime, which is the point at which the quantum anharmonicity should play an important role. For comparison, a full quantum electrodynamical treatment of the coupled system for our particular choice of measurement strategy, including dissipation, but excluding multiple-atom couplings and fluctuations has been carried out [46]. In this treatment, the Jaynes-Cummings resonances discussed in Sec. II A are clearly evident for an atom-cavity system with sufficiently strong coupling when it is probed using a pump-probe geometry similar to that described in this paper. [It should be noted that even for a single atom without fluctuations in number and position, the observation of distinct multiquanta resonances requires a coupling to dissipation ratio of approximately 20, compared to the ratio $2g_0/(\kappa+\gamma_\perp)\approx5$ for this work.] The essential full quantum treatment which includes the effects of multiple atoms with different coupling strengths, of fluctuations in both number and coupling, and of transit effects requires a sophisticated approach, and work is currently underway by Tian and Carmichael [46] to model a system similar to the one described here using the method of quantum trajectories [51]. The computational resources required for such a calculation are large and at present seem too prohibitive to make this a useful technique for detailed quantitative comparison with experimental results.

III. SEMICLASSICAL SIMULATIONS OR WHAT EXACTLY IS A ONE-ATOM EFFECT?

A. Description

We turn now to a discussion of modeling our experiment. At the most fundamental level, we have a complex quantum mechanical system consisting of a beam of atoms interacting with a single cavity mode. Ideally, we would like to make predictions of the outcomes of particular measurements on such a system. A full quantum treatment presents, however, a challenging task. To model our experiment requires keeping track of a phenomenally large amount of information. For example, even when there is on average less than one atom in the cavity-mode volume V_m, the response of a large number of ''spectator'' atoms—those atoms which are weakly coupled due to their location on the skirts of the Gaussian beam waist or those atoms which are near the nodes of the standing-wave field—must be taken into account. Indeed, counterintuitively, it is these very atoms which smooth the otherwise much larger fluctuations in cavity transmission and hence allow any sort of useful observation of single-atom effects. But these spectator atoms make a full quantum mechanical simulation extremely costly.

Our initial approach has been to develop a semiclassical model based on the results of the preceding section which accounts for fluctuations in number and position of atoms within the cavity mode but which approximates transit time effects by a simple modification of $\gamma_\perp$ [as discussed in the context of Eq. (58)]. The model is equivalent to a full quantum treatment in the weak-field linear regime, but is a semiclassical approximation for strong excitation. The semiclassical model starts at Eq. (31) or (58) and proceeds as follows.

We begin with a series of ‘‘tosses’’ of atoms into the cavity mode. Each toss consists of choosing randomly the (x_j, y_j, z_j) coordinates of N_s atoms and evaluating the mode function $\psi(\vec{r}_j) \equiv \psi_j$ for each atom. The simulation volume V_s contains, and is much larger than, a volume of space equal in size to the mode volume V_m. To model our experiments in which the atomic beam is collimated only by the cavity substrates (collimation equal to the length of the cavity transverse to the atomic beam direction), V_s is chosen to be $10w_0$ along the Gaussian waist (x,y directions) and only $l/4$ along the cavity axis (z direction) since this accounts for all possible couplings along the standing wave. For each toss an effective number of atoms, $N_e = \Sigma_{j=1}^{N_s} |\psi_j(\vec{r}_j)|^2$, is calculated. [In addition, $M_e = \Sigma_{j=1}^{N_s} |\psi_j(\vec{r}_j)|^4$ is computed for the nonlinear simulations.] Typically, to achieve $N_e \sim 1$ in V_s, $N_s \approx 100$. Simulations with a larger V_s and N_s (but with the same N_e) have been run, with little change in the resulting spectra, confirming that atoms farther than $10w_0$ from the cavity axis contribute negligibly to the overall probe transmission spectrum. From N_e [and (M_e, n_{u}) if necessary] a transmission spectrum is generated using either Eq. (31) or (58). The transmission function generated with each toss is then averaged over a large number $N_t \sim 2000$ of tosses. Thus, finally produced is an averaged spectrum $Q_a(\omega) = 1/N_t \Sigma_{i=1}^{N_t} t_a(N_{e_i}, M_{e_i}, \omega)$ where t_a is either $|t_{\mathrm{lin}}|^2$ from Eq. (31) or $|t_{\mathrm{nonlin}}|^2$ from Eq. (58). Q_a results from an average collective atom number $N_a \equiv \Sigma_{i=1}^{N_t} N_{e_i}/N_t$. More specific details of the simulations depend on the regime (linear or nonlinear) of simulation and the type of probe detection employed.

B. Linear simulations

We begin with the results of our linear simulations. Equation (31) is used to generate the appropriate transmission function which is then averaged over a large number of tosses to produce Q_{lin}. It is clear that Q_{lin} will not be identical to a spectrum generated by directly inserting N_a into Eq. (31), especially in the case $N_a \sim 1$ when Poissonian fluctuations are relatively large. It could be possible, however, from the definition of N_e and N_a that a given averaged splitting could be equivalently generated either from a few atoms strongly coupled to the cavity mode or from many atoms weakly coupled to the cavity mode. This is actually not true, because the number fluctuations in the two cases leaves observably different signatures on the resultant spectrum as was first pointed out in Ref. [17]. Indeed, in Ref. [17] a convincing measure of the average intracavity atom number is derived from the effects of fluctuations on the linear probe transmission spectrum. Pursuing this issue in more detail, we will compute the distribution of atoms which contributes to a given experimental or simulated spectrum. Particularly, we would like to know the role of a single nearly optimally coupled atom in a spectrum with $N_a \sim 1$. The impact of a single atom in a cavity with the parameters of this experiment is quite large. For example, the cavity transmission on resonance changes by a factor $1/(1+2/N_0)^2 \sim 10^{-3}$ when a single optimally coupled atom traverses the cavity mode, and so one optimally coupled atom is expected to play a very important role in a given spectrum.

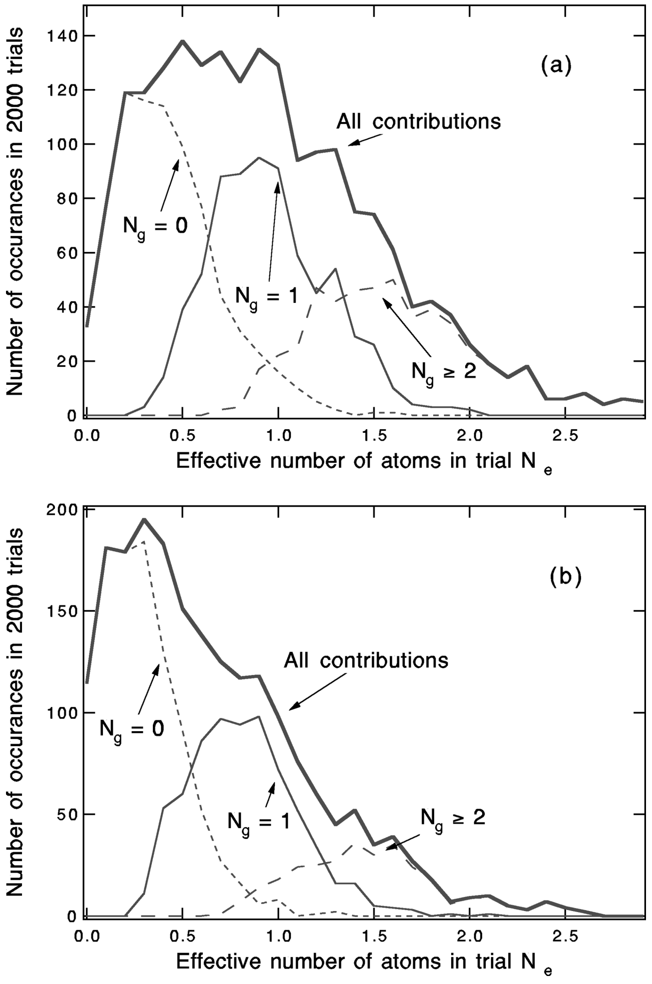

FIG. 3. Occurrences of occupation number N_g in volume $V_g = V_m$ (as discussed in the text) for a typical 2000-trial simulation of $N_a \approx 1.0$ (a) and $N_a \approx 0.7$ (b).

Let us continue this pursuit. We define a volume in which an atom will have a certain fraction of the optimal coupling, say, $g_c = f_c g_0$ [in which case the ‘‘coupling’’ volume $V_g = \epsilon(f_c) V_m$]. Now for each toss of atoms (N_s is chosen to give $N_e \sim 1$) we count the number of atoms N_g in V_g and keep track of those cases in which exactly one atom appears in V_g ($N_g = 1$), when no atoms at all appear in V_g ($N_g = 0$), and when two or more atoms are present in V_g ($N_g \geqslant 2$). The result of such a tracking is histogrammed in Fig. 3 and shown along with the sum of all contributions. Here we make the choice $\epsilon = 1$, corresponding to $V_g = V_m$ and $f_c = 0.56$. We show the distributions for $N_a \approx 1.0$ (a) and

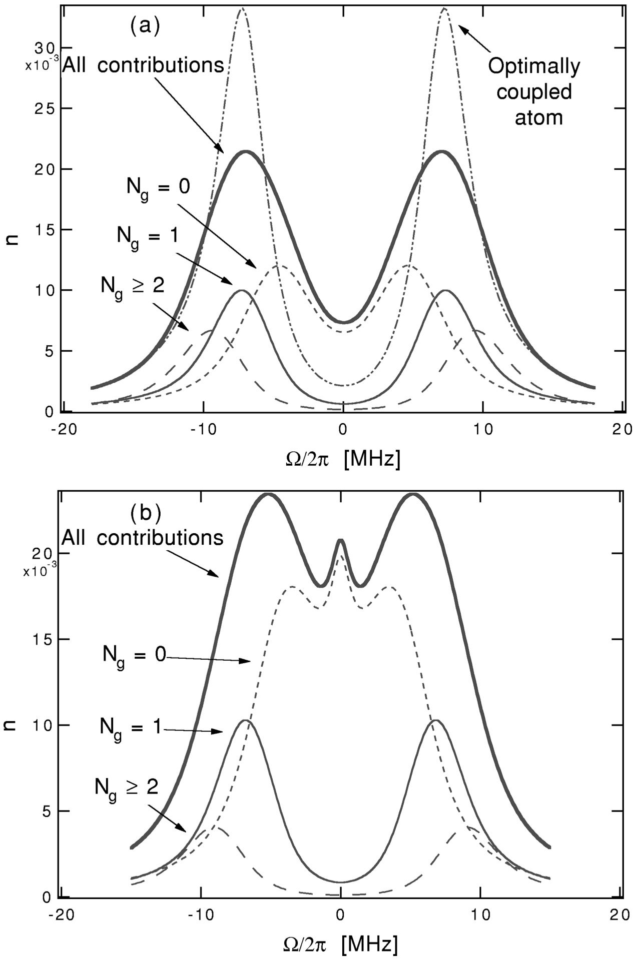

FIG. 4. Breakdown of the contributions of various numbers of atoms in the cavity-mode volume (as discussed in the text) for two different average intracavity atom numbers, corresponding to the histograms of Fig. 3. Graph (a) has $N_a \approx 1$ atom (with the dash–double-dotted curve for one atom optimally coupled for comparison) and graph (b) has $N_a \approx 0.7$ atoms. $(g_0, \kappa, \gamma_{\parallel})/2\pi = (7.3, 0.6, 5)$ MHz, $\gamma_{\perp} = \gamma_{\parallel}/(2\times 0.7)$.

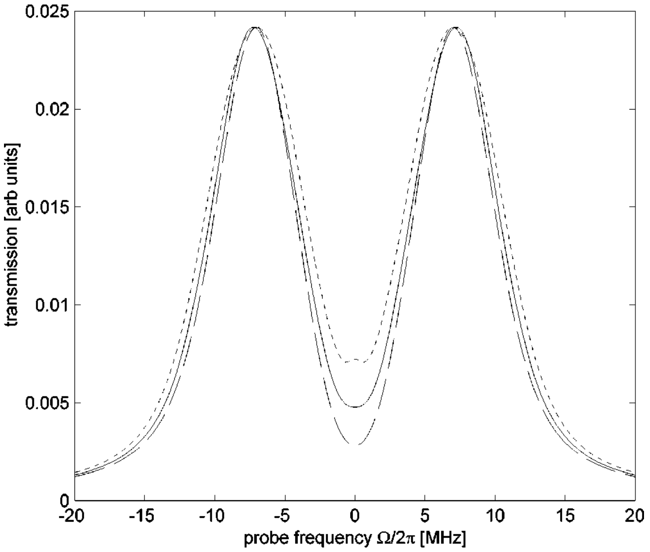

FIG. 5. Comparison of simulated averaged spectra for different numbers of atoms, N_a, with different couplings g_0, such that $g_0\sqrt{N_a}$ is constant. The details are the following: Solid trace, $N_a = 1.0$, $g_0/2\pi = 7.3$. Dotted trace, $N_a = 0.83$, $g_0/2\pi = 8.0$. Dashed trace, $N_a = 1.22$, $g_0/2\pi = 6.6$. For all traces, $\gamma_{\parallel}/2\pi = 5$ MHz, $\gamma_{\perp} = \gamma_{\parallel}/2$, $\kappa/2\pi = 0.6$ MHz. Note the increased role of atomic beam fluctuations as the mean number of atoms, N_a, is decreased, evidenced by the rising central region.

$N_a \approx 0.7$ (b). In Fig. 4 we show the corresponding spectra, with the contributions to the overall probe transmission spectra shown for the same breakdown as in Fig. 3. The contrast of the averaged spectrum with a spectrum due to a single atom optimally coupled to the cavity mode is also shown.

Several comments are in order at this point.

(1) The number of trials in the simulation and the number of spectator atoms N_s are important parameters of the simulation. These must not be chosen too small.

(2) It turns out that the fluctuations allow an independent calibration of the atom number. For example, in the weak-field spectrum (in the absence of beam fluctuations), only the product of the coupling and the number of atoms appears, in the term $g_0\sqrt{N}$. Thus if N increases and g_0 decreases sufficiently to keep $g_0\sqrt{N}$ constant, the spectrum will not change. However, in the case with fluctuations, this is no longer true, essentially because the weight of the contribution of the empty cavity depends on the mean number of atoms, N_a. Thus varying N_a and compensating with g_0 to keep $g_0\sqrt{N_a}$ constant *will not* keep the averaged spectrum the same. The spectra are especially sensitive to the absolute atom number near the center. This is demonstrated in Fig. 5 for N_a varying by 20% around $N_a \sim 1$. Towards a greater emphasis of this point, let us summarize the ideas of the immediately preceding sentences: Perfect linear transmission spectra (that is, in the absence of atomic beam fluctuations) cannot distinguish between a sample of N atoms collectively coupled to the cavity mode at a rate $g_{\text{collection}}\sqrt{N}$ and a single atom coupled to the cavity mode at a rate g_{single} *if* $g_{\text{collection}}\sqrt{N} = g_{\text{single}}$. However, if there are atomic beam fluctuations, the *averaged* spectra in the two cases are different and the single-atom and many-atom cases can be distinguished.

(3) For the two values of N_a shown, the $N_g = 1$ case is a major contributor both to the N_e breakdown (35% of the cases had $N_g = 1$) and to the magnitude of the overall splitting. The overall splitting is indeed given by $g_0\sqrt{N_a}$ to good approximation for $N_a = 1$, slightly less so for $N_a = 0.7$. A further study has shown that the absolute error in splitting as determined from the simple prescription of measuring the peak separation and dividing by $2g_0$ to infer $\sqrt{N_a}$ as compared to the result from the simulation remains approximately constant as the number of atoms is lowered, so that the relative error becomes increasingly large. For example, for the two values of N_a shown in Fig. 4, for the simulation with $N_a = 1$ the splitting is g_0 to within 4%, while for the simulation with $N_a = 0.7$ the splitting is $g_0\sqrt{0.7}$ to 10%. While paradoxically the case for single-atom effects may not be as convincing as for our previous cavity parameters (Ref. [17], with smaller g_0), we are still convinced that what we observe when $N_a \sim 1$ is an effect with unique unambiguous signatures arising from the strong coupling of single atoms within the mode volume V_m. Note that these conclusions do not change significantly for moderate changes of V_g.

(4) It can be seen clearly in Fig. 4(b) that there is an auxiliary peak at $\Omega=0$. The breakdown in terms of the values of N_g shows that this is contributed from those cases in which there are no atoms in V_g—this is simply the transmission function of the (very large) empty cavity peaking through. During the times when there are no atoms in V_g, there are still a large number of spectator atoms giving rise to $N_e \sim 0.4$ from Fig. 3(b). These spectator atoms play the critical role of keeping the empty cavity from completely dominating the transmission spectrum. The central peak can be made much larger by shrinking V_s and thereby lowering N_s as has been done in Ref. [22]. Our choice of V_s is for an atomic beam whose dimensions are much larger than the cavity waist which has the important effect of diminishing the role of the empty cavity while retaining observability of the essential single-atom effects.

It should be noted at this point that this is not a universally accepted interpretation of the situation. The authors of Ref. [22] have argued that there is no way to observe normal-mode splittings in the ‘‘true single-atom regime’’ with presently realized cavity QED parameters. Their point is as follows: Clearly, the actual cavity volume V_c is much larger than our chosen V_g (formally $V_c \rightarrow \infty$), and when $N_e=1$ there is certainly more than one atom interacting with the whole cavity volume (formally $N_s \rightarrow \infty$). If one takes V_g to be much larger than V_m and demands (as a definition of the ‘‘true single-atom regime’’) that at most one atom ever be present in $V_g \gg V_m$, then for an atomic beam experiment in which only the average atomic density can be controlled, most of the time there will be no atoms at all present within V_m. In this case, the single-peaked empty-cavity response will completely dominate the spectrum and no splitting at all will be observable. As this is simply their choice of a *definition* of the ‘‘single-atom regime,’’ it is irrefutable. We should note that a similar viewpoint is adopted in Ref. [32].

Of course, the cavity volume V_c is as large in the transverse dimension as the cavity mirror substrates, and where one draws the formal boundary is somewhat arbitrary. Our choice for this boundary is a reasonable definition based on a volume in space equivalent to the cavity-mode volume, in which the coupling is large ($|\psi|^2 > 0.31$ for $V_g = V_m$). In any event, the breakdown of the spectra (especially those of Ref. [17]) clearly shows that single atoms contribute significantly to the overall spectra and that the ‘‘spectator’’ atoms serve the primary function of attenuating the otherwise large empty-cavity contribution. To define the ‘‘true single-atom regime’’ by demanding that the empty-cavity peak dominate, as Refs. [22,32] have in effect done, may be appropriate in some situations (e.g., the cavity transits described in Ref. [31]) but seems to us not to be physically motivated in the current setting of atomic beam cavity QED. The choice $V_g = V_m$ accounts for 70% of the total cooperativity parameter.

Aside from these issues, there are two points which should be mentioned regarding claims made in Ref. [22]. First we note that the ‘‘unique feature,’’ descibed in their paper (the unique feature being the central peak due to the empty cavity at low atomic beam flux), was observed and described earlier by us, both experimentally [52] and in simulations of the effects of fluctuations in the atomic beam [17]. These are quite well-known effects, and their importance has been amply noted [1]. We also note that their observation of ‘‘line-shape splitting without normal-mode oscillations,’’ might be taken to imply that one can be fooled by ‘‘line-splitting’’ observations. This observation was made in an experiment in which the atom-cavity parameters are not in the strong-coupling limit (the eigenvalues are purely real), and so their observed ‘‘line splitting’’ of course has nothing to do with a normal-mode splitting—in fact it is not a ‘‘line splitting’’ at all but merely the two maxima in the transmission function on either side of the atom-absorption valley, as we measured and noted well before their result [29].

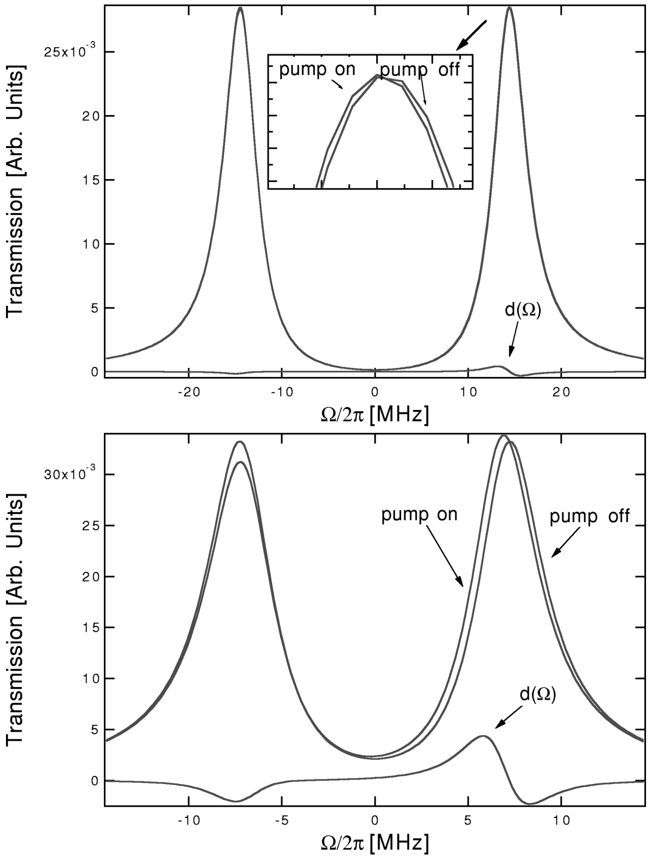

FIG. 6. Calculated nonlinear spectra (strong pump, weak probe) for optimally coupled atoms. Pump power $n_{\mathrm{u}} = n_0/2$ for (a) $N=4$ and (b) $N=1$ optimally coupled atom(s). The frequency of the pump is at $g_0\sqrt{N}$ in both curves. $d(\Omega)$ is the difference spectrum derived by subtracting the spectrum without a pump from the spectrum with a pump. $(g_0, \kappa, \gamma_\parallel)/2\pi = (7.3, 0.6, 5)$ MHz, $\gamma_\perp = \gamma_\parallel/2$.

C. Nonlinear simulations

We first present plots derived directly from Eq. (58) via numerical calculation for optimally coupled atoms. For optimally coupled atoms, $N_e = M_e \equiv N$, the actual number of atoms in the cavity. In order to help quantify the nonlinear effect, we derive a difference spectrum simply by subtracting the pump-absent case from the pump-present case. Figure 6 shows pump on/off transmission spectra along with difference spectra for $N=4$ and $N=1$. We expect expression (58) to be valid only for pump intracavity photon numbers $n_{\mathrm{u}} < n_0$.

The simulation in the nonlinear case is similar, but slightly more complicated than the linear case. As in the linear case, we begin by choosing the *desired* number of atoms, N_d. Of course, we cannot know N_a until the simulation is complete, but if the calculation parameters are chosen appropriately, then we can get N_a consistently close to N_d. We also choose an approximate desired number of intracavity pump photons, n_d, from which we can calculate the appropriate (and approximate) fixed drive by use of the state equation

$$i_{in}=n_d\left[\left(1+\frac{2N_dC_1}{1+d^2+n_d/n_0}\right)^2+\left(\phi-\frac{2N_dC_1d}{1+d^2+n_d/n_0}\right)^2\right], \tag{63}$$

where d and ϕ are defined in the context of Eq. (61). This fixes i_{in} for the entire simulation. As usual, N_e and M_e are computed for each toss. Now, since the the actual pump intracavity photon number n_u builds up depending on the values of N_e and M_e, we must solve Eq. (61) in order to have an appropriate n_{u} associated with the fixed drive i_{in} which can then be used in Eq. (58) for each toss. For consistency of notation, we will call this effective pump intracavity photon number η_e in analogy to N_e and M_e, and likewise, η_e averaged over N_t trials will be called η_a in analogy with N_a. In Figs. 7 and 8 we show histograms of N_e, M_e, and η_e for $N_a=3, \eta_a=n_0/3$, and $N_a=1, \eta_a=n_0/5$, respectively. The corresponding spectra are shown in Fig. 9. For these figures, the pump frequency is coincident with the Rabi peak for the desired number of atoms, N_d. This is a fixed quantity, the same for every toss with value

$$\Delta_{\text{u}}=-\sqrt{N_dg_0^2-\frac{(\gamma_\perp-\kappa)^2}{4}}. \tag{64}$$

In practice, N_a turns out to be very close to N_d $[(N_a-N_d)/N_d<0.01]$, and so indeed Eq. (64) does turn out to be a pump at the correct frequency. This procedure is meant to mimic the experimental situation in which there is an estimate of the number of intracavity atoms (based on the linear transmission spectrum) with the pump detuning set accordingly and with an arbitrary external fixed drive power.

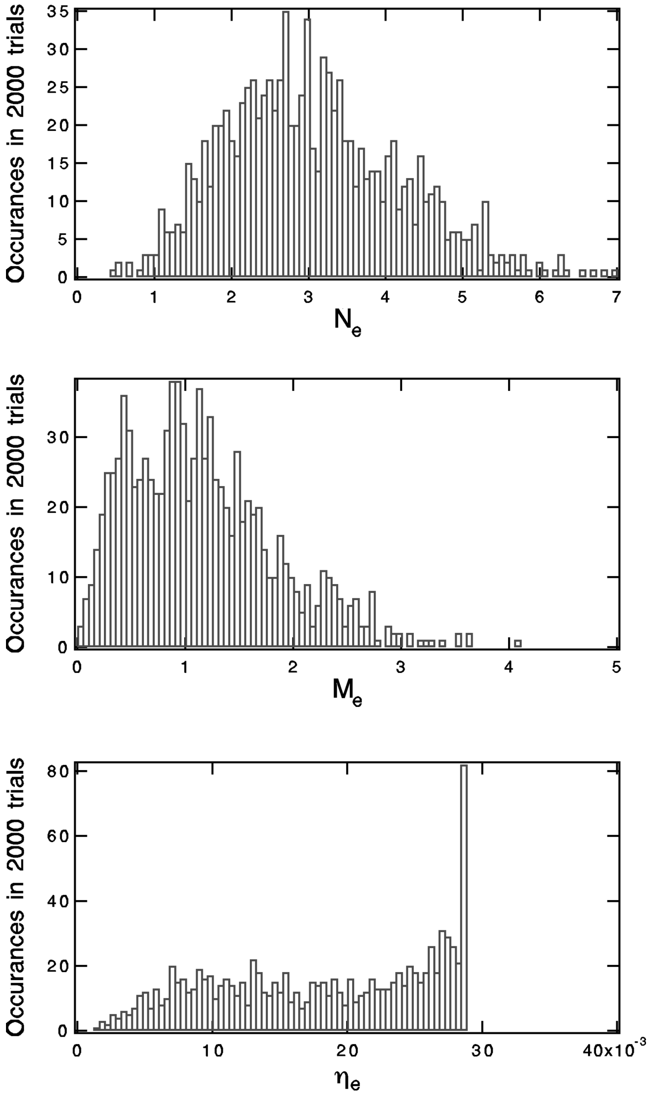

FIG. 7. Histogram of N_e, M_e, and η_e for a full nonlinear simulation ($N_t=2000$) for $N_a\approx 3, \eta_a\approx n_0/3$, and $n_0=0.06$. The abrupt final point in η_e can be explained by the following. There is a fixed drive strength, so that there is clearly a maximum value of η_e allowed. We are driving with the pump at the Rabi peak, and so a fluctuation in atom number in either direction always causes the pump to leave resonance and the buildup to decrease.

D. Comments on comparison of simulated and experimental data

We are free in the simulations to average over the modulus $[Q_a=\overline{|t(\omega)|}^2]$ or the modulus square $[Q_a=\overline{|t(\omega)|^2}]$ of the transmission spectrum. Of course, we can simulate any averaging process, but ultimately we would like to choose one that corresponds most closely to that actually used in an experiment. Unfortunately, this has proved to be slightly more problematic than it may at first appear. We therefore will discuss carefully in this section how a comparison of simulated and experimental data is made.

All results presented thus far are for averaging over the modulus square $[Q_a=\overline{|t(\omega)|^2}]$. An experiment in which this is the correct choice is one which employs a photon-counting detection process. Let us assume that the time scale over which the intracavity atomic distribution evolves is set by the transit time T_0 of atoms crossing the cavity field. Over a time T_0 each atom distribution ''snapshot'' evolves into the next. Our experimental detection always averages over many snapshots, producing the averaged transmission spectrum Q_a. In the case of photon counting, the detector samples for a time $t_d \gg T_0$ during which the cavity-output photon stream is collected. This performs an average over the *intensity* of the cavity-output field so that $Q_{\text{pc}}=\overline{|t(\omega)|^2}$ is measured. This was the detection method of our previous work [17] and the simulations fit well with the data. In addition, we have done a limited number of photon-counting measurements for the cavity parameters of this experiment, and again we have seen good agreement between simulation and data [1]. (To look ahead, refer to Fig. 12.)

The photodetection used in most of the present experiments, however, is different. For the measurements of pump and probe fields, there are two different fields with frequency separation ranging from a few to tens of MHz, and so good frequency discrimination is required (which is quite difficult with photon counting and frequency selective filtering). Detection via an optical heterodyne was therefore utilized. In

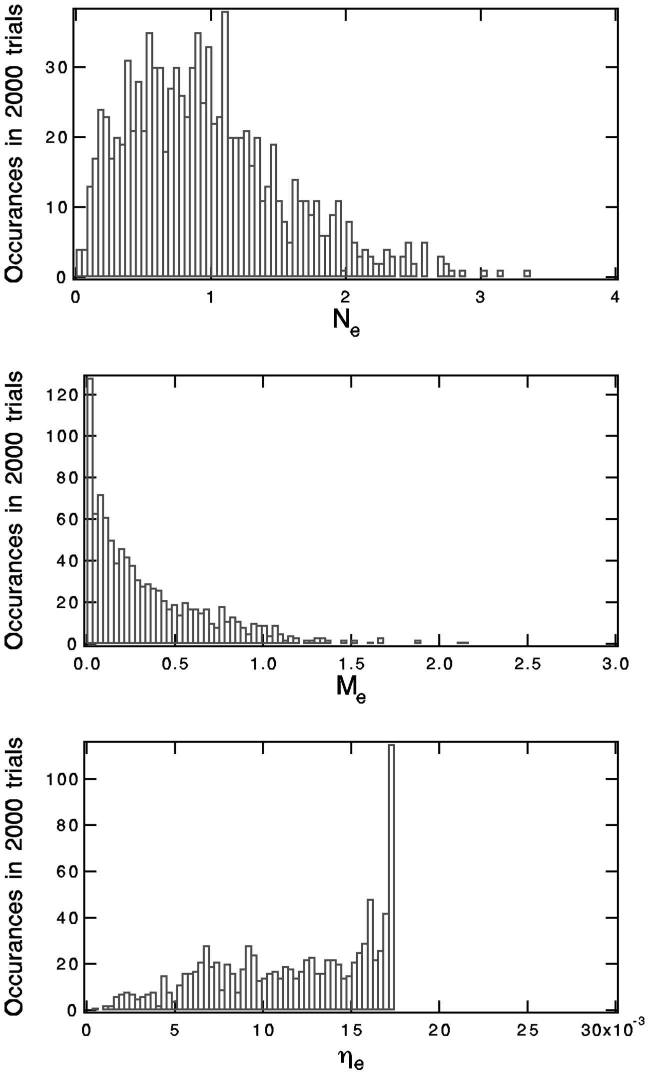

FIG. 8. Histogram of N_e, M_e, and η_e for a full nonlinear simulation ($N_t=2000$) for $N_a \approx 1$, $\eta_a \approx n_0/5$.

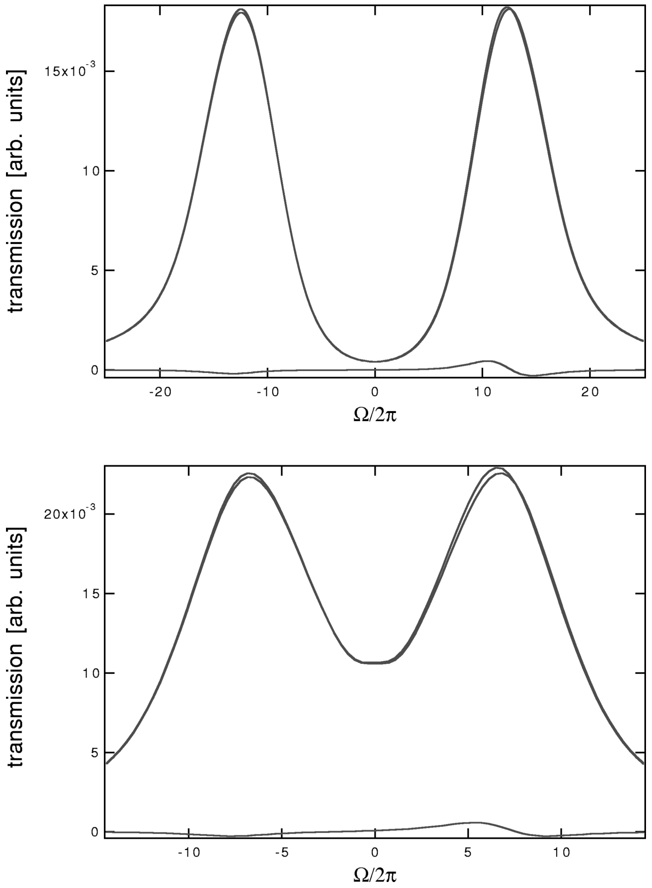

FIG. 9. Spectra associated with Fig. 7 (top graph) and Fig. 8 (bottom graph). $(g_0, \kappa, \gamma_\parallel)/2\pi = (7.3, 0.6, 5)$ MHz, $\gamma_\perp = \gamma_\parallel/(2 \times 0.7)$.

this type of detection, the field *amplitude* of the transmission spectrum is written as coherent modulation on an rf photocurrent in combination with (white) shot noise and noise due to atomic fluctuations. The technique by which this photocurrent is then processed determines the appropriate averaging of the data. Any process seeks to extract the coherent signal from the inevitable noise sources. We chose a sensitive (low-noise-floor) rf spectrum analyzer to mix down the rf and readily view the modulation as a dc signal on the screen of the spectrum analyzer (SA) which is then digitized and stored on a computer. The critical element is the resolution bandwidth (RB) of the SA which was was chosen small, $2\pi B \ll T_0^{-1}$, so that the spectrum analyzer performs an averaging over many atomic transit times. The spectrum analyzer has an envelope detector and not a true square law detector, so that the averaging performed by the spectrum analyzer is of the $\overline{|t(\omega)|}$ type, which we then square in post-processing to produce *in principle* a measurement of $Q_{\text{het}} = \overline{|t(\omega)|}^2$.

Spectra simulated with the two different methods of averaging yield qualitatively similar but quantitatively different line shapes and amplitudes. This is shown in Fig. 10 for two different values of N_a. The differences are by far most pronounced near $\Omega = 0$. This region is also very sensitive in the experiment to uncertainties such as beam alignment. It is an empirical fact that no matter how carefully we have characterized and traced the signal processing elements and the heterodyne detection, on the whole, the data agree better with a calculation of $Q_a = \overline{|t(\omega)|^2}$ than with $Q_{\text{het}} = \overline{|t(\omega)|}^2$. In light of this, we continue to use the $Q_a = \overline{|t(\omega)|^2}$ averaging process in our simulations throughout. While this may seem a brash decision based on our knowledge (both theoretical and for simple empirical test cases) of the inner workings of the heterodyne detection, it turns out not to be critical for several reasons. The first, as we have stated, is that the most pronounced difference between the two averaging procedures appears in the ''valley'' between the Rabi peaks, near $\Omega = 0$. This is a notoriously sensitive region. For example, the auxiliary central peak in Fig. 4(b) is exquisitely sensitive to experimental uncertainties, particularly atomic beam alignment and, indeed, to the fluctuations in atom number themselves. Slight changes in N_a (on levels far more sensitive than our control over oven temperature drift, e.g.) produce dramatic changes in the central peak. Simply put, it is difficult to model the central region of the data successfully. The second saving grace is that the position of the Rabi peaks does not differ to any significant degree for the two methods of averaging as determined from simulations. And, finally, the simulated difference spectra are only slightly affected, perhaps indicating that this simple mathematics (subtraction) reveals the true underlying eigenstructure, which

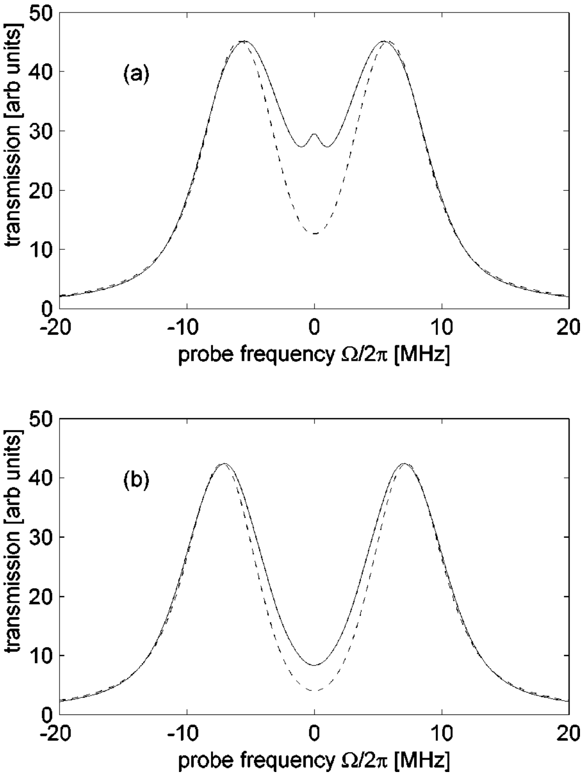

FIG. 10. Comparison of methods of averaging the simulated spectra for (a) $N_a=0.7$ and (b) $N_a=1.0$. In each graph the solid curve is $\langle|t_{\text{lin}}|^2\rangle$ and the dashed curve is $\langle|t_{\text{lin}}|\rangle^2$. The parameters are $(g_0,\kappa,\gamma_\parallel)/2\pi=(7.3,0.6,5)$ MHz, $\gamma_\perp=\gamma_\parallel/2$.

surely must be independent of the way the data are averaged. In particular, the position of the difference peak does not change at all under the two averaging types.

IV. PUMP-PROBE EXPERIMENT

A. Apparatus

The experimental setup employed is as depicted in Fig. 11 [53,54]. The core of the apparatus is a small ($L=346$ μm, $w_0=38$ μm), high-finesse ($\mathcal{F}=3\times10^5$) resonator formed by the two mirrors M_i and M_o with radii of curvature 17 cm and transmission coefficients $\delta_i\approx1\times10^{-6}$ and $\delta_o\approx1.5\times10^{-5}$ (nontransmission scattering losses in the cavity coatings were on the order of 4×10^{-6}). An optically prepared beam of cesium atoms intersects the cavity axis at 90°. The transition investigated is the $(6S_{1/2}F=4,\ m_F=4\rightarrow6P_{3/2},\ F'=5,\ m_F'=5)$ transition at 852 nm. Together with the free-space lifetime of the $6P_{3/2}$ level ($\tau=32$ ns [55]), these parameters lead to the set of rates $(g_0,\kappa,\gamma_\parallel)/2\pi=(7.3\pm0.3,0.6\pm0.1,5)$ MHz. From the above parameters, $(n_0,N_0)=(0.16,0.06)$. Transit broadening due to $T_0\approx10/\gamma_\parallel$ leads to a modification of $\gamma_\perp=\gamma_\parallel/(2\times0.7)$ [50].

The linear response of the coupled atom-cavity system is investigated using a frequency-tunable probe generated using an acousto-optic modulator (AOM) and electro-optic modulator (EOM) from the output of a frequency-stabilized titanium-sapphire laser (10–100 kHz rms linewidth). The probe is mode-matched to the TEM_{00} mode of the cavity, whose length is actively servo controlled to within 10% of its full spectral linewidth. The cavity-length servo consists of a large-intensity ($n_{\text{lock}}\approx10^3n_s$) ''lock beam'' incident on the cavity; both mirrors are on piezoelectric transducers (PZT's) with which the cavity length is dithered very slightly (at 80 kHz; the cavity transmission is changed by the dither by less than 1%). The transmitted lock beam is detected via a lock-in amplifier with the error signal fed back to a mirror PZT. The lock beam is chopped by a mechanical chopper wheel (50% duty cycle at 1.7 kHz) to attain an attenuation of more than 60 dB during the ''off'' cycle, at which time the probe beam is observed without the interference of the lock beam. The transmission of the weak ($n_p\ll n_s$) probe beam is recorded as a function of its frequency on a (rf) SA after balanced optical heterodyning with an intense local oscillator frequency detuned -40 MHz from the common uncoupled atom-cavity center (frequency ω_1 of Fig. 11). For the nonlinear spectroscopic studies, we employ an additional fixed-frequency pump field, which is generated by summing a constant-frequency, variable-strength, rf signal with the tunable, weak, rf probe signal. The resultant sum of rf signals drives the EOM for pump-probe generation.

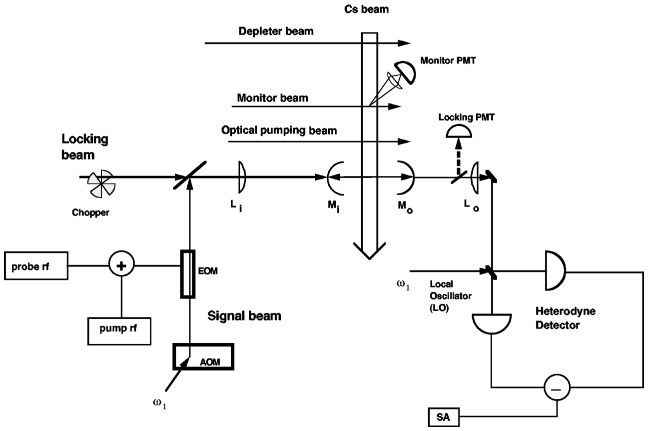

FIG. 11. Schematic of the experimental apparatus. EOM is an electro-optic traveling wave modulator. The depleter beam controls the atomic flux in the correct ($F=4$) ground state, and the monitor beam registers this flux. The locking beam is part of the cavity length servo and is chopped at 1.7 kHz. During the ''off'' cycle of the locking beam, the transmitted probe is measured by the balanced heterodyne detector. L are mode-matching lenses. The reflectivity of the beam splitter which deflects part of the cavity output to the lock photomultipler tube (PMT) is 15%.

B. Linear results

In order to touch base immediately with the Monte Carlo simulations described in Sec. III, we start this section with data taken via a photon-counting method, in which the averaging process is unquestionably of the type $Q_a=\overline{|t(\omega)|^2}$. These data for an average intracavity atom number $\bar{N}=1$ are shown in Fig. 12. The experimental details are identical with those of Ref. [17], and so we will not discuss the details here. Note that we have introduced a new quantity $\bar{N}$. This is the experimentally determined version of N_a from the simulations. As per the discussion above, $\bar{N}$ can be read directly from the measured splitting between Rabi peaks for $\bar{N}\gtrsim1$, but should be determined from a fit to simulations with av-

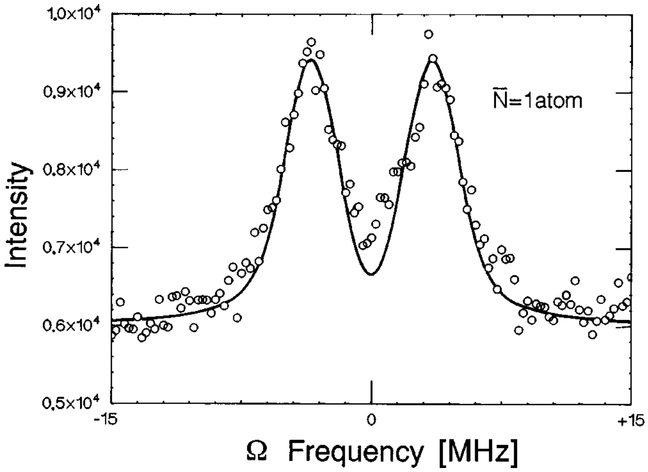

FIG. 12. Linear spectrum for $\overline{N} \approx 1.0$ atoms measured by photon counting with $\omega_a = \omega_c \equiv 0$. The intensity axis is arbitrary. The solid curve is a simulation which includes the effects of atomic number and coupling fluctuations with $g_0/2\pi = 7.3$ MHz and $N_a = 1.0$, $\kappa/2\pi = 0.6$ MHz, $\gamma_\perp/2\pi = 2.5/0.7$ MHz, $\gamma_\parallel/2\pi = 5$ MHz.

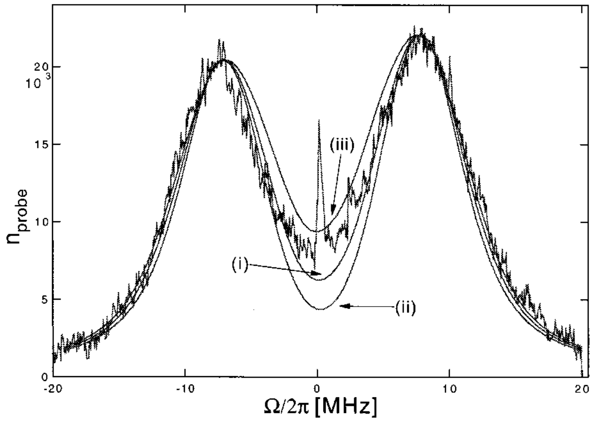

FIG. 13. Linear spectrum for $\overline{N} \approx 1.1$ atoms measured by heterodyne detection. Nominally $\omega_a = \omega_c$, but there is a slight atomic detuning of ≈ -1MHz. The solid curves are simulations which include the effects of atomic number and coupling fluctuations. Curve (i) has $g_0/2\pi = 7.3$ MHz and $N_a = 1.1$; curve (ii) has $g_0/2\pi = 8.0$ MHz and $N_a = 0.95$; curve (iii) has $g_0/2\pi = 6.6$ MHz and $N_a = 1.4$. $\kappa/2\pi = 0.6$ MHz, $\gamma_\perp/2\pi = 2.5/0.7$ MHz, $\gamma_\parallel/2\pi = 5$ MHz.

eraging over fluctuations for atom numbers below this. The procedure of fitting averaged transmission spectra $Q_a = \overline{|t(\omega)|^2}$ is seen from Fig. 12 to work quite well, as expected from our experience with our previous system with smaller g_0. However, it can be seen already in these and related data that the points near $\Omega = 0$ are subject to a larger variance than those elsewhere in the frequency scan. This aspect does not tend to go away by averaging a large number of traces. Rather, imperfections of various sorts (including atomic beam alignment) tend to ''fill in'' the central region which makes it a problematic region for comparisons with the simulations, as stressed above.

We would like to stress at this juncture that the number of intracavity atoms inferred from the measured data depends on the values of $(g_0, \kappa, \gamma_\parallel, \gamma_\perp)$ which are known from independent measurements. For example, κ is determined from both cavity ring-down measurements and by scanning the linewidth directly. The atomic lifetime is known from the literature [55], giving $\gamma_\parallel$; the transverse decay rate $\gamma_\perp$ is determined from the atomic velocity and the well-known cavity waist size [50]. Finally, in addition to the geometric factors, such as the cavity length and cavity waist (which depends on the length and the mirror radii of curvature), g_0 depends on the degree of optical pumping of the atomic beam, since the coupling of any of the other magnetic substates to the cavity field is less than that of the $m_F = 4 \rightarrow m'_F = 5$ transition, which we nominally prepare. There is a straightforward and powerful way of determining the effectiveness of the optical pumping. At reasonably large numbers of intracavity atoms ($\overline{N} \sim 2-4$), we can measure the splitting of the Rabi peaks both with optical pumping and without optical pumping. The average coupling for an atomic sample uniformly populating the magnetic sublevels of the $F = 4$ ground state is determined by an average over the Clebsch-Gordon coefficients connecting each of the allowed transitions. The value of the coupling if all of the atoms were pumped to the $F = 4$, $m_F = +4$ ground state should be $p = 1.73$ times larger than the unpumped sample. Typically we measure $p_{\text{meas}} = 1.6 + 0.1/-0.2$, which is the primary error in the quoted value of g_0 (the rest coming from small contributions from errors in the measured length of the cavity and in the radii of curvature of the mirrors). In principle, an independent measure of the saturation photon number can place additional limits on the value of g_0. The saturation photon number can be measured by observations of the position of the turning points in optical bistability measurements, as was done in our previous measurements [17]. Unfortunately, we were not able to perform reliable bistability measurements with this cavity, mainly due to limitations in attainable intracavity atom number and problems with atomic beam fluctuations.

We now move on to the heterodyne measurements, which are imperative for nonlinear spectroscopy and which are used exclusively onward from this point. We present in Fig. 13 a typical transmission spectrum of the probe beam for our coupled atom-cavity system, in the weak-field limit (with no pump field present). Here $\overline{N} = 1.1$ atom, with $\Omega = 0$ corresponding to the position of the common uncoupled atom-cavity resonance. To facilitate comparison with Eq. (31) the data have been processed by squaring the output of the SA, subtracting the background (shot noise) level, and then normalizing to account for the frequency dependence of the probe generation and detection process [53,54]. Note that the ordinate is normalized in units of the intracavity photon number n_{probe} with $n_{\text{probe}} \lesssim 0.02$ over the scan range (compare this to $n_0 = 0.16$). The observed doublet structure with peaks at $\Omega = \pm g_0$ is a direct spectroscopic measurement of the vacuum-Rabi splitting discussed above. (The sharp feature at $\Omega = 0$ is the rf generated during the lock cycle by the lock beam, a small amount of which feeds through electronic rf attenuators which otherwise prevent this signal from reaching the SA. It is not present during the data taking cycle.)

Also shown in the figure is a series of simulation plots, using the measured values of g_0,κ, and $\gamma_\perp=\gamma_\parallel/2/0.7$. The simulation plots are generated as discussed above in Sec. III. For the parameters of our system, the magnitude of the splitting even in the presence of fluctuations is $g_0\sqrt{\overline{N}}$ with the principle effect of the fluctuations being a significant increase in the cavity transmission near $\Omega=0$. Thus, since g_0 is known independently, we can determine the number of atoms to a good approximation simply by measuring the splitting, but we can also calibrate this procedure by studying the sensitivity of our spectra to atomic beam fluctuations in the vicinity of $\Omega=0$. This is shown with curves (i)–(iii) in which $g_0\sqrt{N_a}$ is kept constant while g_0 and N_a are varied. Curve (i) has $g_0/2\pi=7.3$ MHz and $N_a=1.1$, as we would surmise from the data and the knowledge of g_0, while (ii) has $g_0/2\pi=8.0$ MHz and $N_a=0.95$ and (iii) has $g_0/2\pi=6.6$ MHz and $N_a=1.4$, neither of which match as well as curve (i). As stated above, we have fixed the simulation-averaging procedure at $Q_a=\overline{|t(\omega)|^2}$, which appears to perform quite well. Note that in comparison with our previous measurements [17], the resolution of the splitting for a single atom is significantly improved in our current system, but not by as much as one might naively expect, from the more than twofold increase in the coupling ($g_0/2\pi=3.2\rightarrow7.3$ MHz) and the more than eightfold increase in the single-atom cooperativity parameter C_1. This disappointing result is due to the even greater role of atomic fluctuations in a system with increased C_1.

C. Nonlinear results

Armed with this experience in the linear realm, we next move to explore the nonlinear spectroscopy of the coupled system. We note immediately that our goal in performing the pump-probe-type experiment was to observe multiphoton quantum transitions and to study the evolution of these resonances for large numbers of atoms where the semiclassical equations should correctly predict spectra. If we take Eq. (1) as a guide, we conclude that $\overline{N}=4$ atoms is sufficiently large to be reasonably well described by semiclassical theory, since $q_a=0.94$ for this atom number. In addition, at this number of atoms, the effects of fluctuations in atom number are less pronounced than for $\overline{N}\sim1$. To recapitulate our objective, consider the transitions (t_0,t_1) and (t_0^*,t_1^*,t_2^*) shown in Fig. 1. We are most interested in the transition t_1. For a system with a single optimally coupled atom in which $g_0\gg(\kappa,\gamma_\perp)$, this would appear in the nonlinear spectrum as a peak centered at frequency $(\sqrt{2}-1)g_0$ relative to the atom-cavity center frequency ω_0. The transition t_0 is strongly suppressed relative to t_1, and so we will not search for it. In our system, which is more complicated, due to atomic beam fluctuations, and not sufficiently enough split for this ideal picture to be realized, we should consider not the ideal case of Eq. (2), but rather the case of Eq. (13) and the associated transitions (t_0^*,t_1^*,t_2^*) generalized to the distributed atoms case. Again, the transitions (t_0^*,t_2^*) are strongly suppressed relative to (t_1^*), and so our goal will be to trace this transition as we lower the intracavity atom number $\overline{N}$. If our choice of measurement (which will be the position of the peak in the difference spectrum) turns out to be an accurate reflection of the transition frequencies, then we should be able to trace out data similar to the calculated quantities shown in Fig. 2.

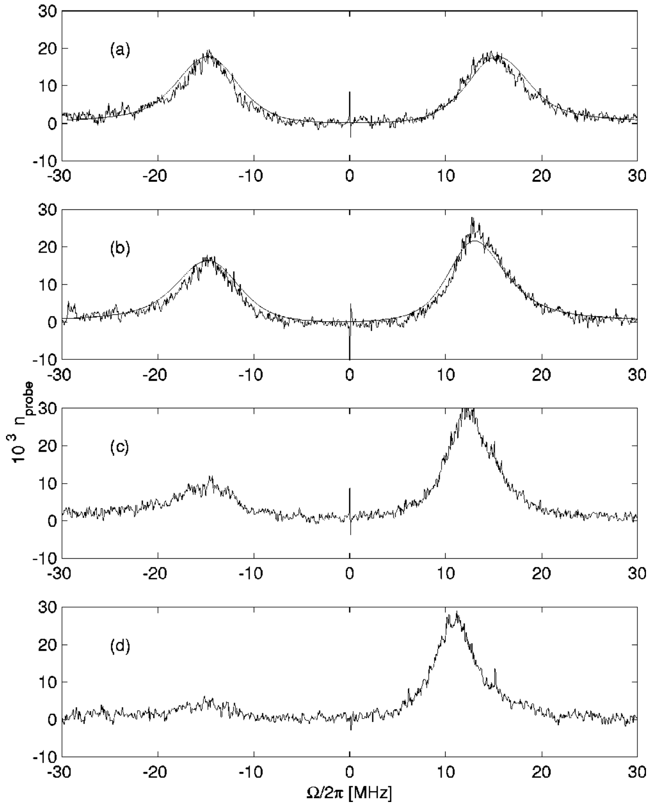

FIG. 14. Sequence of nonlinear probe spectra for $\overline{N}\approx4.2$ atoms with $\omega_a=\omega_c\equiv0$. Here, the frequency Ω of a constant amplitude probe beam is swept and the transmission recorded (in units of probe intracavity photon number $n_{\rm probe}$). Trace (a) has a probe field only, with the solid curve a fit to the data including the (minimal) effects of atomic fluctuations. From (b) to (d), the pump powers (again in units of intracavity photon number with atoms present) are $\overline{\eta}\approx0.1$, 0.3, 0.8. The pump frequency is $\Omega_{\rm pump}/2\pi=g_0/2\pi\sqrt{\overline{N}}=14.8$ MHz, as indicated by the sharp feature in trace (d). The solid line in trace (b) is a nonlinear semiclassical simulation including atomic fluctuations and is described in the text. The best fit to the data has $\eta_a=0.38$.

In Fig. 14 we present a sequence of pump-probe spectra, with varying pump intensity, taken for a ''large'' number of atoms ($\overline{N}=4.2$ atoms). The experimentally measured pump intracavity photon number $\overline{\eta}$ ranges from zero intracavity pump photons to $\overline{\eta}=0.75\pm0.3$ intracavity photons, on average, and its frequency is chosen to coincide with the higher-frequency resonance of the unpumped atom-cavity system at $\Omega/2\pi=+(g_0/2\pi)\sqrt{\overline{N}}=14.8$ MHz [this is visible as a sharp peak in the data, especially of graph (d)]. The data have been processed in the same manner as in Fig. 13. For trace (a), taken with no pump, the observed splitting is just that of the weak-field normal-mode splitting discussed previously. From the fit (solid curve) and the splitting, we find that $\overline{N}=4.2$, with the only adjustable parameter being the overall vertical scaling. In trace (b) the pump has been turned on, with a pump intensity corresponding to approximately $\overline{\eta}=0.1\pm0.05$ intracavity photons, while in (c) the pump has

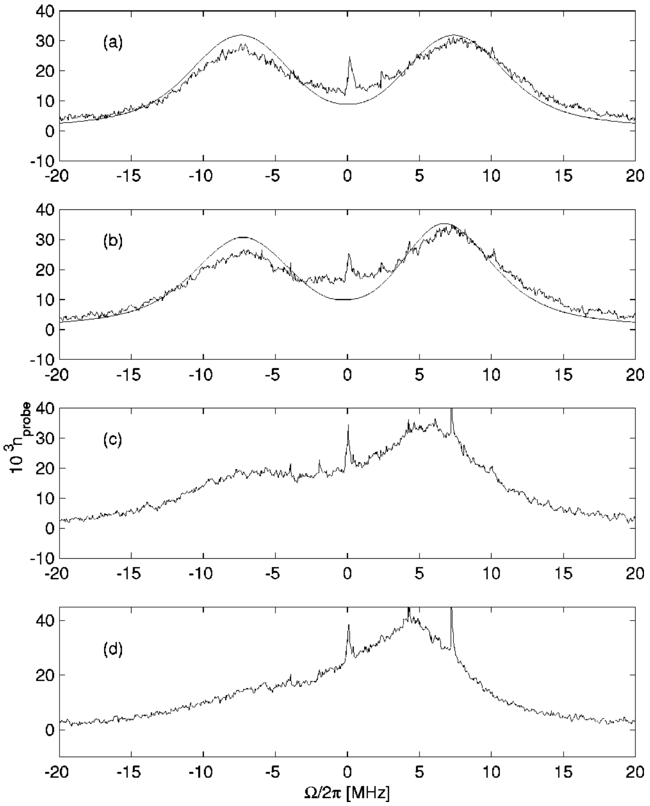

FIG. 15. Sequence of nonlinear spectra for $\bar{N}\approx 1.1$ atoms with $\omega_a=\omega_c\equiv 0$. Graph (a) has a probe field only. The pump powers are from (b) to (d), $\bar{\eta}\approx 0.1$, 0.4, 0.7 intracavity photons on average. The pump frequency is $\Omega_{\rm pump}/2\pi=g_0/2\pi\sqrt{\bar{N}}=7.6$ MHz, as indicated by the sharp feature in trace (d). The solid curves are semiclassical simulations with $N_a=1.1$, and for graph (b) $\eta_a=0.07$. See the text for a discussion.

been increased to $\bar{\eta}=0.4\pm 0.2$ photons and finally in (d) the pump is at $\bar{\eta}=0.75\pm 0.3$ photons. Clearly evident from the data is a trend towards lower heights for the ''unpumped'' peak as the pump power is increased. At the same time the pumped peak becomes higher and migrates inward towards the common atom-cavity frequency at $\Omega=0$. In addition, the width of the ''pumped'' peak narrows, with the width of the upper peak in graph (d) being 30% reduced compared to that of the peak in graph (a). In each case the pumped peak is higher than the unpumped peak and no additional resonances are observed. For a linear system, the probe response would be independent of the pump (except of course at $\Omega_{\rm probe}=\Omega_{\rm pump}$), so that the data in Fig. 14 represent a measurement of the nonlinear ''susceptibility'' for the atom-cavity system. The solid curve in trace (b) is a theoretical fit from Eq. (58) averaged over atomic distributions using the numerical simulation technique described above. Here the average atom number and overall height are parameters of the simulation, with N_a having been set from the fit in (a) to $N_a=4.2$ and likewise for the height found in (a). The pump intensity is then the only free parameter for the fit to the nonlinear case, yielding a value for the intracavity pump intensity of $\eta_a=0.38$ photons which is high compared to the measured value of $\bar{\eta}=0.1\pm 0.05$.

We next turn to data taken for approximately one intracavity atom. Figure 15 shows a sequence similar to Fig. 14 for

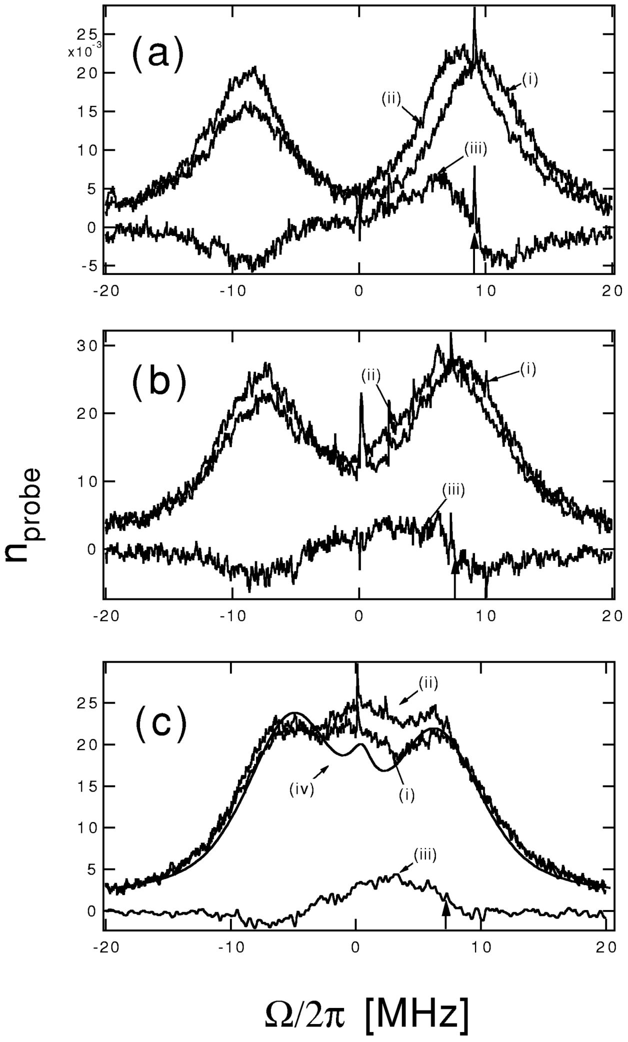

FIG. 16. Linear and nonlinear spectra as the number of atoms is varied. Each graph contains a linear (no pump) spectrum [curve (i)], a nonlinear spectrum [curve (ii)], and a difference spectrum [curve (ii) - curve (i)] [curve (iii)]. From top to bottom the parameters are: (a) $\bar{N}\approx 1.6$, $\bar{\eta}\approx 0.4$, $\Omega_{\rm pump}/2\pi=9.1$ MHz; (b) $\bar{N}\approx 1.1$, $\bar{\eta}\approx 0.2$, $\Omega_{\rm pump}/2\pi=7.5$ MHz; (c) $\bar{N}\approx 0.75$, $\bar{\eta}\approx 0.06$, $\Omega_{\rm pump}/2\pi=7.2$ MHz. Curve (iv) in graph (c) is a theoretical fit to the linear spectrum, indicating the extent to which our Monte Carlo simulations correctly incorporate fluctuations in atom number and position. As stated in the text the region near $\Omega=0$ is extremely sensitive to imperfections in the apparatus, including atomic beam alignment, but these factors should remain constant between the linear and nonlinear spectra measurements.

$\bar{N}\approx 1.1$ atoms. The solid curves are again from numerical simulations of the semiclassical theory applied to the data in the same manner as in Fig. 14. It is seen that the linear simulation in this case is not as good a fit as that of Fig. 14, for the following reason. The data are taken under conditions in which the cavity and atomic detunings are nominally zero, but are subject to some drift ($\sim\pm 0.1$ MHz cavity detuning and $\sim\pm 1$ MHz atomic detuning), as has happened in the case of Fig. 15. We do not at present model such detunings in our nonlinear simulations. In order to determine an approximate height scaling of the nondetuned linear simulation which can then be applied to the nonlinear simulation, we leave the detunings out of the linear fit as well. It is clear that

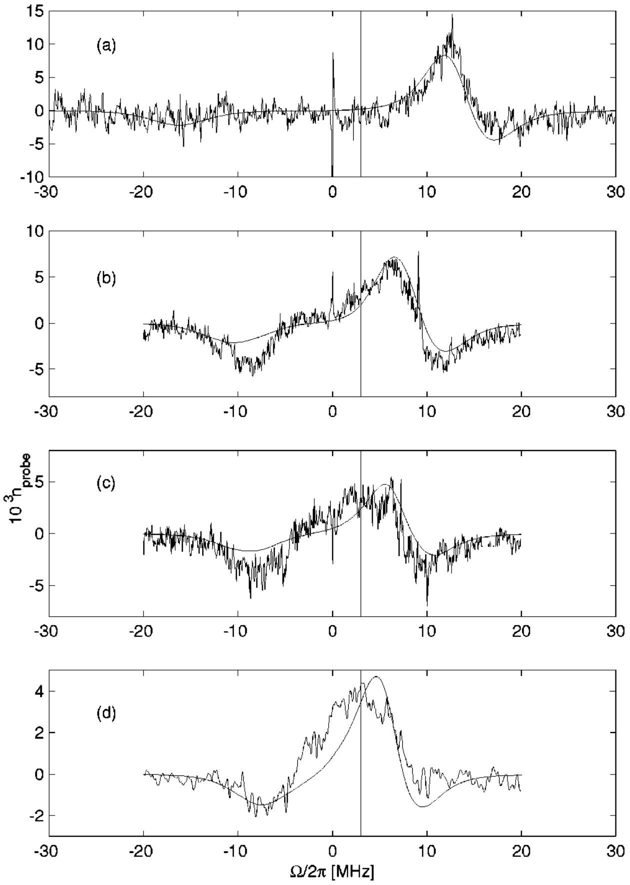

FIG. 17. Difference spectra with semiclassical theory overlaid. The details are the following: Trace (a), $\overline{N}=4.2$, $\overline{\eta}=0.1$, $N_a=4.2$, $\eta_a=0.38$. Trace (b), $\overline{N}=1.6$, $\overline{\eta}=0.4$, $N_a=1.6$, $\eta_a=0.16$. Trace (c), $\overline{N}=1.1$, $\overline{\eta}=0.1$, $N_a=1.1$, $\eta_a=0.07$. Trace (d), $\overline{N}=0.75$, $\overline{\eta}=0.06$, $N_a=0.75$, $\eta_a=0.09$. Data are taken with the pump frequency at $\Omega_{\rm pump}/2\pi=g_0\sqrt{\overline{N}}$ for $\overline{N}\geqslant 1$ and at $\Omega_{\rm pump}/2\pi=g_0$ for $\overline{N}<1$. The solid vertical lines depict the position of the transition t_1 at $(\sqrt{2}-1)g_0$.

this procedure is nonoptimal, but it does reproduce the qualitative features of the nonlinear data. The pump powers for Fig. 15 are similar to those in Fig. 14. The best fit for pump photon number in Fig. 15(b) is $\eta_a=0.07$ as compared to the measured value $\overline{\eta}=0.1$. As is obvious from these data, multiquanta resonances of the sort predicted by Fig. 1 are not immediately apparent. As the probe frequency is scanned to investigate the first- to second-excited-state transitions, it of course also probes the ground- to first-excited-state transitions. Thus a means to isolate the nonlinear effect is needed.

In Fig. 16 we introduce a naive attempt at such a technique by simply subtracting the linear spectrum from the spectrum with the pump field present, thereby deriving a ''difference'' spectrum from the data, much the same as the difference spectrum from the nonlinear simulations shown in Figs. 6 and 9. The difference spectrum contains much information. For example, one may look for additional features that arise in a regime where the basic first-excited-state features change little. This would be indicated by near complete subtraction of the linear features with a new peak appearing at a frequency different from that of the pump frequency. Figure 16 shows linear (i), nonlinear (ii), and difference spectra (iii) as $\overline{N}$ is decreased from $\overline{N}\approx 1.6$ to $\overline{N}\approx 1.1$ to $\overline{N}\approx 0.75$. Here we have selected the data based on a level of a qualitatively similar magnitude for the nonlinear effects.

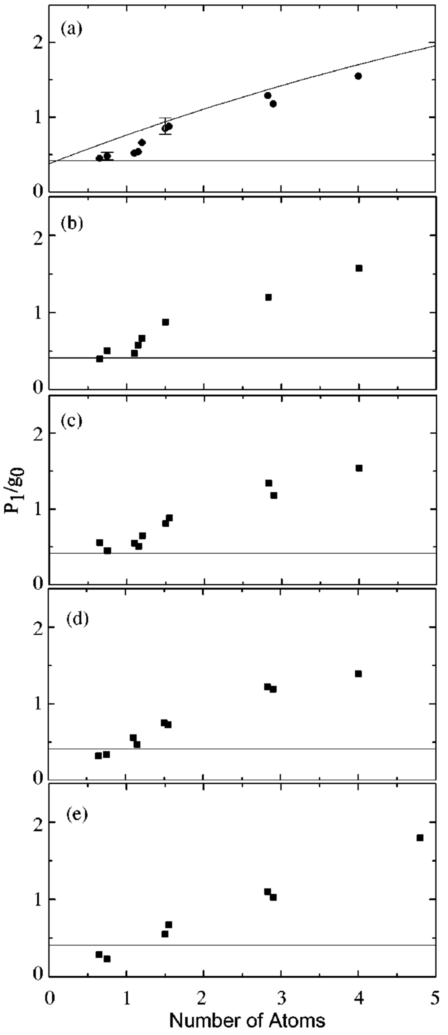

FIG. 18. Plot of the position of the peak in the difference spectrum P_1/g_0 vs the number of intracavity atoms (N_a for simulations or $\overline{N}$ for the data). The data are shown as the open squares while the simulation results are represented by the solid curve in graph (a), which is a fit through many runs of the nonlinear simulation to show the trend of the semiclassical prediction. The data of graph (a) are taken with intracavity pump photon numbers in the range $0.06<\overline{\eta}<0.2$. Note the suggestive flattening of the data at $(\sqrt{2}-1)$ (the position of the peak corresponding to the transition t_1 in Fig. 1, shown as the horizontal straight line) perhaps indicative of a quantum anharmonicity. Data are taken with the pump frequency at $\Omega_{\rm pump}/2\pi=g_0\sqrt{\overline{N}}$ for $\overline{N}\geqslant 1$ and at $\Omega_{\rm pump}/2\pi=g_0$ for $\overline{N}<1$. The ranges of pump powers for the subsequent graphs are (b) $0.06<\overline{\eta}<0.1$, (c) $0.1<\overline{\eta}<0.2$, (d) $0.2<\overline{\eta}<0.4$, and (e) $0.5<\overline{\eta}<0.9$. The error bars displayed represent the one-standard-deviation limits, and are shown on only two points to avoid clutter.

The data of Fig. 16(c) are data taken with $\overline{N}\approx 0.75$ atoms. Here the pump frequency is at $\Omega/2\pi=g_0/2\pi=7.2$ MHz. Note that three peaks are evident in both the probe-only data and in our linear numerical simulation [curve (iv)], with the central peak arising from the fact that now there is a significant fraction of the time in which there are no atoms present within the cavity-mode volume. This a promising regime, because the contribution from multiple atoms in the cavity-mode volume should be small (see Sec. III), while the response from the zero-atom contribution (i.e., atoms outside the mode volume V_m with coupling $g<\epsilon_c g_0 \approx 0.56 g_0$) should be essentially linear since the saturation intensity is higher for these ''spectator'' atoms (because they are each weakly coupled). Thus an observed nonlinear response should be predominately due to contributions from single intracavity atoms within the mode volume. Of course, the trade-off is that the peaks have merged to a degree that may drastically obscure the observation of new features. What we observe in the pump-probe spectra is a region of increased probe transmission, again on the inner side of the pumped peak, with very little change in the position or height of the unpumped peak or of the outer side of the pumped peak. Clearly evident in the difference spectrum is a broad peak centered roughly at $(g_0/2\pi)(\sqrt{2}-1)=3$ MHz, which is consistent (but certainly not compellingly so) with what one expects from the QED theory of Sec. II A (not including atomic fluctuations). That there are only small dips below zero at the positions of the pump-off resonances indicate that there has been only minor modification of the single-quantum resonances. We emphasize that the peak shown in the figure demonstrates a nonlinear response for a system containing just one atom (on average) and an intracavity photon number of only $\bar{\eta}\approx 0.1$ photons.

While the data shown in Fig. 16(c) are suggestive, we should stress that without a QED calculation which models all aspects of our experiment, including atomic transit effects and the critical role played by fluctuations in the atomic number and position, it is difficult to determine the extent to which the data of Fig. 16 can be explained by a semiclassical model (including the proper treatment of transit effects) or whether there are aspects which have a purely quantum origin.

To further quantify our observations, we present in Fig. 17 difference spectra with a corresponding set of simulated difference spectra from our semiclassical model. The pertinent information can be found in the figure caption. Unfortunately, these data and their comparison with simulations does not shed much more light on the issue of multiquanta resonances. However, they do show that the semiclassical simulations qualitatively agree with the data at ''large'' numbers of atoms ($\bar{N}=4.2$) tending towards lesser agreement with the smaller atom numbers, though any quantitative comparison is far from conclusive. Whether this trend is indicative of a fundamental disagreement between a semiclassical theory and the experiment or due to complications of the experiment such as transit broadening is certainly not easy to determine. It is possible that the features that we seek are to be found in a parameter regime not covered by the simulations. In fact, most of the data that we have taken [e.g., Figs. 14(c),(d) and 15(c),(d)] have pump intracavity numbers that are too large for the analytical approximations that went into the derivation of Eq. (58), so that we have no way to compare these data with any theory.

Nonetheless, we continue our pursuit of a quantum feature manifest in the spectra of the atom-cavity system by focusing in on a particular property of the data: the position of the peak on the high-frequency side of the difference spectrum which from Fig. 1 should coincide with the transitions t_1 and t_1^*. Actually, it is an interesting question as to the extent to which the position of the difference peak actually corresponds to the eigenvalues discussed in Sec. II A. From simulations, we find that the position of the difference peak tracks the distributed, averaged eigenvalue [$\langle d_1 \rangle$ from Eq. (18)], but that the latter is about 25% larger. The position of the peak in the difference spectrum is thus not an exact measure of the eigenvalue of the atom-cavity system, but is certainly a related quantity.

The peak in the difference spectrum is a quantity which can be easily measured and simulated, providing another way of comparing the semiclassical Monte Carlo simulations with the actual data. As stated above, this quantity is insensitive to such parameters of the simulation as overall height and applied pump power, making for an easier comparison with experimental data taken over a range of pump and probe powers. In Fig. 18 we accumulate some of the nonlinear data that we have taken for this experiment and plot the positions of the measured peaks in the difference spectra (□) versus the average number of atoms, $\bar{N}$, where we have averaged together data for the measured peak position taken over a range of pump powers from $\bar{\eta}=0.06$ to 0.2 photons. We also show the prediction from our nonlinear semiclassical simulations, represented by a curve that is derived by a fit to many trials of the simulation over a dense collection of atom numbers. (The simulations show that the position of the difference peak is not a strong function of the pump power over the range we consider, even though the height of peaks is.) An interesting feature of the data is a ''kink'' occurring near $\bar{N}\approx 1.3$, followed by a leveling off of the peak position at a level close to $(\sqrt{2}-1)g_0$, for $\bar{N}<1$. The data appear to approach the semiclassical theory at high atom numbers, as we expect, but there are deviations at low atom numbers, with no ''kinks'' observed in the semiclassical theory. It should be noted that most of the low-atom-number data include the semiclassical result near the limits of the uncertainty of the measurement. The leveling of the difference peak position would certainly be a compelling result from our perspective, but again, it is very difficult to determine whether this represents a true quantum behavior given the uncertainties in the peak positions and the caveats associated with our semiclassical simulations.

V. CONCLUSIONS AND THE FUTURE

We have performed extensive measurements of the nonlinear response of a strongly coupled atom-cavity system. While our initial objective was to observe clear multiphoton resonances as a decisive measure of the quantum nature of the system, it appears that our atomic beam system is not optimal for this purpose and allows us to obtain only limited information. In the case of the structural investigation presented here, explicitly quantum aspects of our strongly coupled cavity QED system have hidden behind the mask of Poissonian fluctuations in atom number and position. While we have observed a discrepancy between our measurements and the semiclassical predictions, it is not clear whether this is the result of effects omitted from our model (e.g., transit time) or whether it arises from a real quantum underpinning. For small $\bar{N} \lesssim 1.3$, the evidence is suggestive of the underlying quantum anharmonicity, while for large $\bar{N}$, the data asymptote to the expected semiclassical result. More conclusive data are, no doubt, desirable.

Towards this end we are developing two strategies which we hope will correct the most serious defects of the current atomic beam system. One involves precisely locating the atoms to the strong parts of $\Psi(\vec{r})$ [56] along with timing information of the atomic transit across the cavity mode. The other involves the use of atom trapping techniques [31].

ACKNOWLEDGMENTS

This research is supported by the National Science Foundation and by the U.S. Office of Naval Research.

---

[1] H. J. Kimble, in *Cavity Quantum Electrodynamics*, edited by P. Berman (Academic Press, Boston, 1994), pp. 203–266.
[2] A. Ekert, in *Atomic Physics 14*, Proceedings of the 14th International Conference on Atomic Physics, edited by D. W. Wineland, C. E. Wieman, and S. J. Smith, AIP Conf. Proc. No. 323 (AIP, New York, 1995), p. 450.
[3] A. S. Parkins, P. Marte, P. Zoller, and H. J. Kimble, Phys. Rev. Lett. **71**, 3095 (1993).
[4] A. S. Parkins *et al.*, Phys. Rev. A **51**, 1578 (1995).
[5] C. K. Law and J. H. Eberly, Phys. Rev. Lett. **76**, 1055 (1996).
[6] C. K. Law and H. J. Kimble, J. Mod. Opt. **44**, 2067 (1997).
[7] C. Monroe *et al.*, Phys. Rev. Lett. **75**, 4011 (1995).
[8] D. Meschede, H. Walther, and G. Muller, Phys. Rev. Lett. **54**, 551 (1985).
[9] G. Rempe and H. Walther, Phys. Rev. Lett. **58**, 353 (1987).
[10] G. Rempe, F. Schmidt-Kaler, and H. Walther, Phys. Rev. Lett. **64**, 2783 (1990).
[11] M. Brune *et al.*, Phys. Rev. Lett. **65**, 976 (1990).
[12] F. Bernadot *et al.*, Europhys. Lett. **17**, 33 (1992).
[13] M. Brune *et al.*, Phys. Rev. Lett. **72**, 3339 (1994).
[14] G. Raithel, O. Benson, and H. Walther, Phys. Rev. Lett. **75**, 3446 (1995).
[15] M. Brune *et al.*, Phys. Rev. Lett. **77**, 4887 (1996).
[16] G. Rempe *et al.*, Phys. Rev. Lett. **67**, 1727 (1991).
[17] R. J. Thompson, G. Rempe, and H. J. Kimble, Phys. Rev. Lett. **68**, 1132 (1992).
[18] G. Rempe *et al.*, in *Atomic Physics 13*, edited by H. Walther, T. W. Hansch, and B. Neizert, AIP Conf. Proc. No. 275 (AIP, New York, 1992), p. 305.
[19] G. Rempe, R. J. Thompson, and H. J. Kimble, Phys. Scr. **T51**, 67 (1994).
[20] H. J. Kimble *et al.*, in *Atomic Physics 14* (Ref. [2]), p. 314.
[21] K. An, J. J. Childs, R. R. Dasari, and M. S. Feld, Phys. Rev. Lett. **73**, 3375 (1994).
[22] J. J. Childs *et al.*, Phys. Rev. Lett. **77**, 2901 (1996).
[23] R. J. Brecha *et al.*, J. Opt. Soc. Am. B **3**, 238 (1986).
[24] R. J. Brecha *et al.*, J. Opt. Soc. Am. B **12**, 2329 (1995).
[25] M. G. Raizen *et al.*, Phys. Rev. Lett. **63**, 240 (1989).
[26] Y. Zhu *et al.*, Phys. Rev. Lett. **64**, 2499 (1990).
[27] G. S. Agarwal, J. Opt. Soc. Am. B **2**, 480 (1985).
[28] M. Brune *et al.*, Phys. Rev. Lett. **76**, 1800 (1996).
[29] Q. A. Turchette, R. J. Thompson, and H. J. Kimble, Appl. Phys. B: Photophys. Laser Chem. **60**, S1 (1995).
[30] Q. A. Turchette *et al.*, Phys. Rev. Lett. **75**, 4710 (1995).
[31] H. Mabuchi, Q. A. Turchette, M. S. Chapman, and H. J. Kimble, Opt. Lett. **21**, 1393 (1996); C. J. Hood *et al.* (unpublished).
[32] H. J. Carmichael, P. Kochan, and B. C. Sanders, Phys. Rev. Lett. **77**, 631 (1996).
[33] B. C. Sanders, H. J. Carmichael, and B. F. Wielinga, Phys. Rev. A **55**, 1358 (1997).
[34] E. T. Jaynes and F. W. Cummings, Proc. IEEE **51**, 89 (1963).
[35] M. Tavis and F. W. Cummings, Phys. Rev. **170**, 379 (1968).
[36] P. R. Rice and H. J. Carmichael, J. Opt. Soc. Am. B **5**, 1661 (1988).
[37] P. Alsing and H. J. Carmichael, Quantum Opt. **3**, 13 (1991).
[38] L. A. Lugiato, in *Progress in Optics*, edited by E. Wolf (Elsevier Science Publishers B. V., Amsterdam, 1984), Vol. 21, p. 71.
[39] H. J. Carmichael, Phys. Rev. A **33**, 3262 (1986).
[40] H. J. Carmichael, *An Open Systems Approach to Quantum Optics* (Springer-Verlag, Berlin, 1993).
[41] G. V. Varada, M. Sanjay-Kumar, and G. S. Agarwal, Opt. Commun. **62**, 328 (1987).
[42] G. S. Agarwal, P. K. Bullogh, and N. Nayak, Opt. Commun. **85**, 202 (1991).
[43] C. M. Savage, Phys. Rev. Lett. **63**, 1376 (1989).
[44] L. Tian and H. J. Carmichael, Quantum Opt. **4**, 131 (1992).
[45] J. I. Cirac, H. Ritsch, and P. Zoller, Phys. Rev. A **44**, 4541 (1991).
[46] L. Tian and H. J. Carmichael (unpublished); H. J. Carmichael (private communication).
[47] P. D. Drummond, IEEE J. Quantum Electron. **QE-17**, 301 (1981).
[48] G. S. Agarwal, Phys. Rev. Lett. **53**, 1732 (1984).
[49] M. Xiao, H. J. Kimble, and H. J. Carmichael, Phys. Rev. A **35**, 3832 (1987).
[50] A. T. Rosenberger, L. A. Orozco, H. J. Kimble, and P. D. Drummond, Phys. Rev. A **43**, 6284 (1991).
[51] L. Tian and H. J. Carmichael, Phys. Rev. A **46**, R6801 (1992).
[52] H. J. Kimble, G. Rempe, R. J. Thompson, and R. J. Brecha, in *Laser Spectroscopy: TENICOLS 1991*, edited by M. Ducloy, E. Giacobino, and G. Camy (World Scientific, Philadelphia, 1992), p. 211.
[53] R. J. Thompson, Ph.D. thesis, The University of Texas at Austin, 1994 (unpublished).
[54] Q. A. Turchette, Ph.D. thesis, California Institute of Technology, 1997 (unpublished).
[55] O. S. Heavens, J. Opt. Soc. Am. B **51**, 1058 (1961). More recent measurements show a lifetime of $\tau = 30.5$ ns. See R. J. Rafac *et al.*, Phys. Rev. A **50**, R1976 (1994). Other uncertainties in the experiment (such as our approximate accounting for transit broadening) dominate the difference between this value and the one which is used elsewhere in this article.
[56] O. Carnal, Q. A. Turchette, and H. J. Kimble, Phys. Rev. A **51**, 3079 (1995).